REMOVAL OF SELECTED HEAVY METALS THROUGH MAGNETIC GRAPHITIC CARBON NANO STRUCTURES FROM DRINKING WATER SAMPLES OF THE VARIOUS AREAS OF BALOCHISTAN

Mohammad Shoaib Khan[1*], Manzoor Iqbal Khattak[2], Nida Kazmi[3], Adnan Afridi[4], Munnaza Saeed[5], Hamid Ullah[6]

[1-5]Chemistry Department, University of Balochistan, Quetta - Pakistan
[6-] Chemistry Department, Balochistan University of Information, Technology, Engineering and Management Sciences, Quetta - Pakistan

*Corresponding Author: Manzoor Iqbal Khattak
Email address: manzoor_iqbal@yahoo.com

Abstract

The purpose of the current research is to ascertain the levels of heavy metal pollution in drinking ground water samples taken from various areas of Balochistan, Pakistan. Drinking water contamination is a relatively recent issue that has led to a rise in stress as a consequence of recent enormous population expansion, urbanization, and industry. Because heavy metals are poisonous, persistent, and bioaccumulative in the environment, they are regarded as serious pollutants. Additionally, a brand-new adsorbent was made to extract heavy metals from drinking water. After that, the size and surface morphology of the produced adsorbents were examined using a scanning electron microscope (SEM), and the crystalinity was verified using an X-ray diffractometer (XRD). The elemental analysis of iron and oxygen in the EDX data was followed by TG/DTA characterisation to ascertain its thermal stability. In the province of Balochistan, the maximum samples were determined to be under the limits for heavy metal pollution; nevertheless, the drinking water samples from the Jaffarabad and Zhob districts had the highest zinc contents, measuring 36.24 and 31.00 ug/L, respectively. Thermodynamic characteristics showed that the adsorption of heavy metals was endothermic and spontaneous. The spontaneous character of the process is signified by the negative values of different temperatures as well as shows high affinity of the heavy metals towards the prepared adsorbent

Keywords: Heavy Metals; Nanotechnology; Environmental Pollution; Drinking water,

1. Introduction

Clean and safe drinking water is important component to humans and other living beings for survival of on earth as water quality has direct impact on public health (Kumar, 2003; Mishra et al., 2013). Ground water provides water to introduce to industries, agricultural uses and daily use purposes by the peoples all around the world. Because drinkable surface water is scarce, ground water is becoming more and more important. Because of the protective soil cover that surrounds. Eighty percent Thef infections worldwide are caused by lack of fresh water (drinking water contaminated) and poor sanitation according to the World Health Organization (Versari et al., 2002). In recent times, there has been a noticeable shift in the quality of ground water, with significant pollution occurring as a result of physical, chemical, and biological factors

(Elizabeth et al., 2005; Singh, 2006). There could be metals or other compounds that are harmful to human health even in the absence of anthropogenic pollution (Rao & Mamatha, 2004). Researching human health requires analyzing natural water for various chemical and physical characteristics as well as trace element levels (Mishra & Bhat, 2008). As a result, monitoring and assessing the quality and contamination of ground water is crucial (Sarkar & Banerjee, 2006; Mayur et al., 2007). As of right now, only 80% of people living in urban areas and 11% in rural regions have access to piped water supplies (Khalown, 2004; Cheema,). It has been predicted that one third of the world's population typically uses groundwater for drinking (UNEP, 1999). However, groundwater supplies are vulnerable to pollution from both organic and inorganic contaminants as a result of the sharp rise in industry and population growth. The majority of urbanized and industrialized regions are examples of locations where serious problems with water quality are noted (Khan, 2011). Additionally, waste water from companies containing organic & inorganic stuff are released into the environment directly into developing nations (Forstner & Witman, 1981; Tanji & Valoppi, 1989;Campbell & Tessier, 1991; Zayed et al., 1992).

In dry regions with a high population density, water resources are few or nonexistent, particularly in developing nations like South Africa, which is recognized as a water-scarce nation (Scott, 2000). The global population's need for freshwater is putting pressure on water treatment and purification systems to be managed effectively, economically, and with simple operating technologies (Schwarzenbach et al., 2010; Rodriguez-Reinoso et al., 1997; Wyatt & Linton, 1988).

Three primary categories of water exist: natural, contaminated, and cleansed water.

• Surface water from rain, groundwater, ocean, rivers, streams, springs, and lakes are all considered natural water sources.

• Sewage, sullage, and industrial effluents are examples of contaminated water.

• Potable, distilled, or treated water is considered purified water.

1.1. Heavy Metals

Metals make up a significant portion of contaminants, which are mostly naturally occurring, widely dispersed elements that have been taken from the earth's crust and used industrially for the benefit of humankind. It is well recognized that inorganic chemicals, particularly metals. At the moment, environmental compartments including air, sediment, soil, and water are rich in metals and inorganic ions. Certain inorganic metals, like as sodium, copper, and iron, are essential for life and have a major impact on how well the important enzyme systems operate. Nonetheless, many metals are considered xenobiotics due to their harmful effects on living things, including humans, and their lack of significance in human physiology (Safe, 1994; Rodriguez et al., 2000). This category of metals includes lead, mercury, cadmium, arsenic, and others. Even though metals that are considered necessary may be dangerous when exposed to high amounts of them (Hayward, 1999).

Around 2 billion people do not have free access to clean, safe water, which has a detrimental impact on their health, according to a WHO report (Rodriguez-Reinoso et al., 1997; Wyatt & Linton, 1988; Safe, 1994; Rodriguez et al., 2000; Hayward, 1999). Due to water shortages in developing nations, factors such as deforestation, urbanization, river damming, loss of wetlands, mining activities, agriculture, energy consumption, and unintentional water contamination from oil spills are making it harder for people to acquire fresh water. According to Hayward (1999), all of these have increased pollution and destroyed water catchment regions.

1.2. Adsorption

The adsorption process is a renowned equilibrium separation procedure and has been known to be superior compared to other processes respect of flexibility, initial cost, simplicity of design, insensitivity to toxic pollutants and easy to operate . According to Encinar et al. (2005) selecting the right adsorbent is essential for a successful water treatment procedure in adsorption operations. According to Encinar et al. (2005), adsorbents include, but are not limited to, AWR (Rapant & Krcmova, 2007; Chen, 2002); biomass (Chen, 2002;Velea et al., 2009); AC (Emmanue et al., 2009;Robinson et al., 2002a); low-cost adsorbents of industrial by-products (Vasudevan et al., 2003; Loukidou et al., 2003); clays (Hu et al., 2003;Pereira et al., 2003); polymeric materials (Organic polymeric resins) (Rivera-Utrilla et al., 2003; Lopez et al., 2003); macro porous hyper-

cross linked polymers (Gupta et al., 2003); silica beads (Al-Asheh & Duvnjak, 1997); and zeolites (Shen, 2002).

1.2.1 Activated carbon

Activated carbon is a kind of microporous material. Many carbonaceous (carbon-rich) materials, including wood, coal, coconut shell, peat/lignite, lignin, and agricultural waste residue (AWR), may be used to make activated carbon. The reason activated carbon may adsorb substances is because of the high specific surface area (SSA) of its microporous carbon. Its massive SSA is the primary factor that allows it to remove a great deal of contaminants and impurities in a very tiny limited space. the power to change activated carbon's surface in a manner that modifies its adsorption capacity (Zhang et al., 2003). Activated carbon may be altered in a variety of ways, depending on the application, to increase its surface accessibility. Typically, an activation phase is followed by the surface modification of activated carbon. Three classifications exist for the modification: physical, biological, and chemical.

1.3 Applications of Nanomaterial's in purification of water

Advancements in nanotechnology have produced materials with a high surface area to volume ratio that eliminate harmful metals (Atia et al., 2003). On the other hand, the issue of nanoscale material stability and aggregation limited its practical and prospective uses. It has been stated that these issues may be resolved by encasing nanoparticles in polymer matrix (Pan et al., 2003;Ghoul et al., 2003). Many reports of nanomaterial stabilized polymer matrices for water purification exist, however more research is still needed to fully understand how these materials disperse in polymer matrices (Bosso & Enzweiler, 2002). The relevance of stabilizing nanoparticles and their many prospective uses have been studied in-depth by Yan et al. (Kornaros & Lyberatos, 2006). If the component qualities of the polymer nanostructures are optimized, they may effectively remove heavy metals from wastewater (Nuria et al., 2010).

Many writers have used magnetic adsorbents as alternatives, but they haven't gained much traction because of their small surface area. Therefore, there is an urgent need to find adsorbents that have both surface area and magnetic characteristics so they can remove pollutants with ease.

This research assessed the presence of heavy metals in drinking water around the Province of Balochistan in Pakistan. The sample collection process included selecting districts from throughout Balochistan at random. The study was conducted at the PCSIR Labs Complex in Peshawar, Pakistan, and the Pakistan Council of Research in Water Resources' PCRWR laboratory.

2. Experimental
2.1 Samples Collection

By the year 2022, drinking water samples were being collected in triplicate from each source in the chosen districts of Quetta, Turbat, Jafferabad, and Zhob in Balochistan, using the dry and clean 600 ml plastic sampling bottles.

2.1.1 Framework for Number and size of Samples

Uniform criteria were used for the collection of drinking water samples. Considering this, permanent public drinking water sources were favored. Table 2.1 provides the specifics of the sample
.

Table 2.1: Data of selected districts of sources of water samples

S. No	District Name	District Code	Grid Size (Km²)	Total no of Sources
13.	Quetta	QUE	4	50
14.	Turbat	TUR	2	50
15.	Jaffarabad	JFD	1	50
16.	Zhob	ZHB	1	50

2.3 Heavy Metals Analysis

Using a conventional approach, the Atomic Absorption Spectrophhotometer AOAC 2000 was used to assess heavy metals (Srinivasan and Viraraghavan, 2010). The atomic absorption spectrophotometer's operating settings are listed below, and table 2.2 lists the metal parameters.

Table 2.2: The various wavelengths used for quantification of selected metals are mentioned as follows:

Metals	Wavelength(nm)
As	193.7
Pb	283.3
Cr	357.9
Cu	240.7
Zn	213.9

2.4 Iron-oxide nano-structures preparation

Melon and watermelon waste from Noshki and Dalbadin, Balochistan, were used to create iron oxide nanostructures. After cutting the watermelon and melon waste peels into pieces and drying them, they were placed in BDH solution for a whole day. After being extracted from the solution, the biomass was allowed to air dry at room temperature. Pyrol fumigation was applied to the dry material for 48 hours in order to facilitate pyrolysis. The dried matter that had been treated with pyrolysis was then burned in an assembly (Figure 2.1).
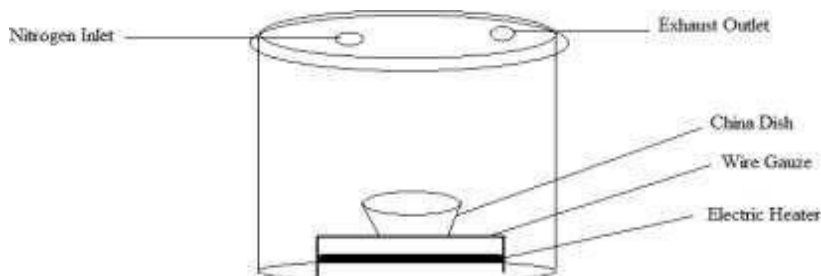
Figure 2.1: Iron oxide nanostructures are created in a specifically made chamber (Wan et al., 2007).

2.3 Iron oxide carbon nanostructure characterization
2.3.1. Surface Area Analyzer

Surface area and porosity are the most important physical parameters, along with material quality and function. Changes in these two factors have a significant impact on the materials' activity. A 0.1

g sample was weighed and analyzed using an American-made Surface Area Analyzer (Zahoor & Khan, 2014).

2.3.2 Using XRD to characterize iron oxide carbon nanostructures
Using an X-Ray Diffracto-meter (XRD) in accordance with a published approach, the X-ray diffraction study of magnetic carbon nanostructures was performed (Zahoor & Khan, 2014).

2.3.3. FTIR characterization of carbon nanostructures containing iron oxide
The field of Fourier Transform Infrared Spectroscopy (FTIR) studies the interaction of electromagnetic radiation with chemical substances. The way electromagnetic radiations interact depends on a substance's characteristics. Consequently, when electromagnetic radiation passes through a material, certain frequencies are absorbed by the molecules, causing molecular vibrations. It should be remembered that each molecule has a unique frequency at which it absorbs electromagnetic radiation, which results in the properties of that particular material (Gong et al., 2012). IR spectra were obtained using FTIR analysis by different scanning ranges.

2.3.4 SEM characterization of carbon nanostructures containing iron oxide
When an electron beam strikes a sample's surface and is reflected back toward the recorder, it creates a picture. This process is known as reflecting light microscopy, or SEM for short. With SEM, a material's surface morphology, including size and shape, may be assessed down to a few nanometers (Zahoor & Khan, 2014).
The sample's topography was evaluated using a SEM grid, and the sample (made in the USA) was coated in gold using a sputter coater running at 30 mA for two minutes. The surface morphology pictures were then captured using a 20 KV SEM (Joel JSM-5910).

2.3.5 Use of TG and DTA to characterize iron oxide carbon nanostructures
The mass of a sample was measured using thermogravimetric analysis (TG), which recorded temperature and time increases in a controlled environment (Zahoor & Khan, 2014).
Using aluminum trioxide as a standard, the produced adsorbents were subjected to TG/DTA analysis of the diamond series manufactured in the United States.

3.2.6. Using EDX to characterize iron oxide carbon nanostructures
This kind of microscopy is used to analyze a substance's chemical makeup, which mostly relies on the sample's interaction with the atoms of the material and electrons. Because each element in the periodic table has a different electron structure, the interaction of a high-energy electron with the material atom produces a distinct X-ray spectrum in EDX spectroscopy. The tiny aluminum stub of the EDX, was placed on a double-sided adhesive tap that was already filled with a dispersed particle that had been sprinkled on (Zahoor & Khan, 2014

2.4. Determination of Kinetic parameters
Using the usual Strokea et al. approach, the kinetics of heavy metal adsorption were carried out (Baby & Ramaprabhu, 2010). A series of 25 ml flasks was obtained, and to get a 200 ppm concentration, a known quantity of heavy metal salts was applied. The produced adsorbent was then added to each flask at a concentration of 0.5% (W/V), and it was arbitrarily spun at a speed of 300 revolutions per minute while maintaining a temperature of 25ºC. After that, a magnetic bar was used to separate the sorbents in each flask. An atomic absorption measurement was performed after the solution had been filtered through Whatman No 1.

2.5 Parameters of adsorption determination
A flask (25 ml) series were used to generate standard heavy metal concentrations of 150, 175, 200, 225, 250, 275, 300, 325, and 350 ppm. After that, these flasks were shaken for 480 minutes at room

temperature on an orbital shaker set at 300 rpm. After that, a magnetic bar was used to separate the sorbents in each flask. A final Whatman No. 1 filter was used to filter the mixture.

2.6. Parameters of thermodynamic determination
The same experimental conditions as described in section 2.5 was used, with the exception that each series' temperatures were fixed for 240 minutes.

2.7. Statistical Analysis in Practice
The collected findings were submitted to analysis of variance, descriptive analysis, and ANOVA utilizing a fully randomized system using the most recent version of SPSS. This package's T-test was used to verify the mean difference.

3 Results and Discussion
3.1 Analysis of heavy metals
According to Stroka et al. (2000) and Baig et al. (2009), heavy metals are persistent, poisonous, and harmful to humans and the environment. They pollute surface and ground water and lower the quality of water that is used for irrigation and drinking. Heavy metals and chemicals that are emitted from many anthropogenic sources have become worldwide issues due to their contamination of drinking water. Freshwater pollution has increased since 1990 as a result of unusual population growth, a rise in industry, and urbanization (Hall et al., 1999; Liu & Kim, 2009). This contamination poses a risk to public health and the environment (Sundarajan & Ramalakshmi, 2012; Kahani et al., 2007). The health risks associated with drinking water contaminated with heavy metals, may arise from both geological and anthropogenic causes. Ore deposits, rocks, and volcanic eruptions are the geogenic sources of metals (Giles et al., 1960).

Global lead pollution is caused by industrialization, namely by car emissions and industrial operations. This is particularly true in major metropolitan centers where there are a lot of automobiles on the road. Because of its serious or hazardous potential for the environment and living things, lead is considered a toxic contaminant.

Chromium (Cr) is used in a variety of sectors, including the tanning of leather, glass and ceramics, paints and pigments, fungicides, and catalyst design. In order to sustain the proper metabolism of glucose in human nutrition, drinking water must include a certain ratio of Cr. When a level is higher than the advised ranges, serious health issues such nephritis and glycosuria might develop (Toth, 1995).

Table 3.1: Permissible Limits of Heavy Metals by various organizations

Heavy Metals	Pakistan EPA Limits (mg/L)	Canadian Limits (mg/L)	United States Limits (mg/L)	WHO Limits (mg/L)
As	0.05	0.05	0.01	0.01
Pb	0.05	0.01	0.01	0.01
Cr	0.5	0.05	0.01	0.05
Cu	2	1	1.3	2
Zn	5	5	5	5

Table 3.2: ANOVA for Arsenic (µg/L) in drinking water collected from selected districts of Balochistan.

Arsenic Balochistan				
Source	Df	MS	F	P
Districts of Balochistan	3	0.00123	9.20	0.0000
Error	196	0.00013	-	-
Total	199	-	-	-

df = degree of freedom,   F = variance ratio

Table 3.3: Arsenic concentration in portable water collected from selected sources of selected districts of Balochistan.

Districts of Balochistan	Arsenic (µg/L) Balochistan				95% LC	
	No of sample	Minimum	Maximum	Mean ± SEM	Lower	Upper
Quetta	50	1.306 E-04	9.307 E-03	9.224E-04[b] ±1.857E-04	5.493 E-04	1.295 E-03
Jaffarabad	50	0.0000	0.0537	0.0111[a] ±1.386E-03	8.340 E-03	0.0139
Turbat	50	0.0000	0.0310	8.702E-03[a] ±1.121E-03	6.447 E-03	0.0110
Zhob	50	0.0000	0.0996	0.0116[a] ±2.728E-03	6.153 E-03	0.0171

Table 3.3 displays the ANOVA results for the mean arsenic concentrations across all Balochistan districts. The results show that there was a significant difference (0.000). The average amounts of arsenic found in the samples taken from several Balochistani areas showed a significant variation (P≤0.05) with a F value of 9.20.

Table 3.4: ANOVA for Lead (µg/L) in drinking water collected from selected districts of Balochistan.

Lead Balochistan				
Source	Df	MS	F	P
Districts of Balochistan	3	5.657 E-06	6.89	0.0002
Error	195	8.211 E-07	-	-
Total	198	-	-	-

df = degree of freedom,   F = variance ratio

Table 3.5: Lead concentration in portable water collected from selected sources of selected districts of Balochistan

Districts of Balochistan	Lead (µg/L) Balochistan				95% LC	
	No of sample	Minimum	Maximum	Mean ± SEM	Lower	Upper
Quetta	50	0.0000	6.510 E-03	5.571E-04[a] ±1.901E-04	1.751 E-04	9.391 E-04
Jaffarabad	50	0.0000	4.370 E-03	6.087E-04[a] ±1.709 E-04	2.652 E-04	9.522 E-04
Turbat	50	0.0000	0.0000	0.0000[b] ±0.0000	0.0000	0.0000
Zhob	50	0.0000	0.0000	0.0000[b] ±0.0000	0.0000	0.0000

Table 3.4 indicates that there was a significant difference of 0.0002 in all samples. The average lead concentration in samples taken from several Balochistan districts showed a significant variation (P≤0.05) with a F value of 6.89.

Table 3.6: ANOVA for Chromium (µg/L) in drinking water collected from selected districts of Balochistan

Chromium Balochistan				
Source	Df	MS	F	P
Districts of Balochistan	3	1.239 E-04	2.16	0.0940
Error	194	5.733 E-05	-	-
Total	197	-	-	-

df = degree of freedom,   F = variance ratio

Table 3.7: Chromium concentration in portable water collected from selected sources of selected districts of Balochistan

Districts of Balochistan	Chromium (µg/L) Balochistan				95% LC	
	No of sample	Min	Max	Mean ± SEM	Lower	Upper
Quetta	50	0.0000	0.0000	0.0000^b ±0.0000	0.0000	0.0000
Jaffarabad	50	0.0000	0.0843	$2.851E-03^{ab}$ ±1.713E-03	-5.902 E-04	6.293 E-03
Turbat	50	0.0000	0.0215	$3.596E-03^a$ ±7.191E-04	2.150 E-03	5.041 E-03
Zhob	50	0.0000	0.0320	$2.708E-03^{ab}$ ±1.087E-03	5.198 E-04	4.897 E-03

The ANOVA for the mean chromium concentrations is shown in Table 3.6. It indicates that there was a significant difference of 0.0940 across all the samples that were obtained from various districts in Balochistan. The average chromium concentrations of the samples taken from several Balochistan districts showed a significant variation (P≤0.05) with a F value of 2.16.

The findings shown in Table 3.7 demonstrated a statistically significant variation in the average chromium content between the samples obtained from the Quetta district and those from the Jaffarabad, Turbat, and Zhob districts.

Table 3 .8: ANOVA for Copper (µg/L) in drinking water collected from selected districts of Balochistan

Copper(Cu) Balochistan				
Source	Df	MS	F	P
Districts of Balochistan	3	0.0000	M	M
Error	194	0.0000	-	-
Total	197	-	-	-

df = degree of freedom,   F = variance ratio

Table 3 .9: Copper (Cu) concentration in portable water collected from selectedsources of selected districts of Balochistan

Districts of Balochistan	Copper(Cu) (µg/L) Balochistan				95% LC	
	No of Sample	Minimum	Maximum	Mean ± SEM	Lower	Upper

Quetta	50	0.0000	0.0000	0.0000 ±0.0000	0.0000	0.0000
Jaffarabad	50	0.0000	0.0000	0.0000 ±0.0000	0.0000	0.0000
Turbat	50	0.0000	0.0000	0.0000 ±0.0000	0.0000	0.0000
Zhob	50	0.0000	0.0000	0.0000 ±0.0000	0.0000	0.0000

There was significant difference (0.0000) in the copper concentrations across the several districts in Balochistan, according to the ANOVA of Table 3.8. With the value of F=M, copper was found to be substantially different in all districts (P≤0.05). Table 3.9 showed that there were no appreciable differences in the copper levels found in the samples taken from each district in Balochistan.

Table 3.10: ANOVA for Zinc (µg/L) in drinking water collected from selecteddistricts of Balochistan

Zinc (Zn) Balochistan				
Source	**Df**	**MS**	**F**	**P**
Districts of Balochistan	3	948.735	21.2	0.0000
Error	194	44.697	-	-
Total	197	-	-	-

df = degree of freedom,   F = variance ratio

Table 3.11: Zinc (Zn) concentration in portable water collected from selected sources of selected districts of Balochistan

Districts of Balochistan	Zinc(Zn) (µg/L) Balochistan				95% LC	
	No of sample	**Minimum**	**Maximum**	**Mean ± SEM**	**Lower**	**Upper**
Quetta	50	0.0000	23.410	3.4373^b ±0.8116	1.8062	5.0684
Jaffarabad	50	0.0000	36.240	11.156^a ±1.4519	8.2371	14.076
Turbat	50	0.0000	12.650	1.9474^b ±0.5476	0.8464	3.0484
Zhob	50	0.0000	31.000	2.0400^b ±0.7543	0.5242	3.5558

Table 3.10 displays the ANOVA of Zinc for every district in Balochistan. The average zinc levels in the samples taken from various Balochistan districts showed a significant difference (P≤0.05) with a F value of 21.2.

Table 3.11 makes it clear that the mean zinc content of the samples taken from the district of Quetta differed significantly from the samples taken from the district of Jaffarabad.

3.2 Iron oxide nanostructures preparation

Watermelon and melon (peel) waste were combined to create magnetic adsorbent in a specially built chamber, as illustrated in Fig. 3.1. By exposing the produced adsorbent to the magnetic bar, its magnetic characteristics were observed.

3.2.1 The Prepared Adsorbents' Characteristics

The following advanced instruments were used to characterize the produced adsorbents:

3.2.2 Surface Area Analyzer characterization of the synthesized adsorbents

The magnetic adsorbent's surface area and pore distribution were depicted in Figures 3.2, 3.3, 3.4, and 3.5, respectively, while Tables 3.12 and 3.13 displayed various surface characteristics of the adsorbent that was created.
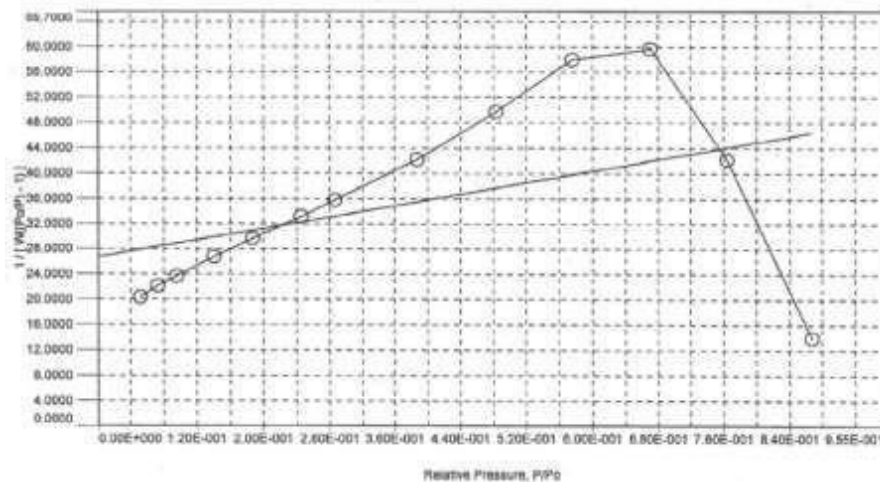
Figure 3.2. Graph showing BET surface area of the prepared iron oxide carbon nanostructures from Water Melon waste.
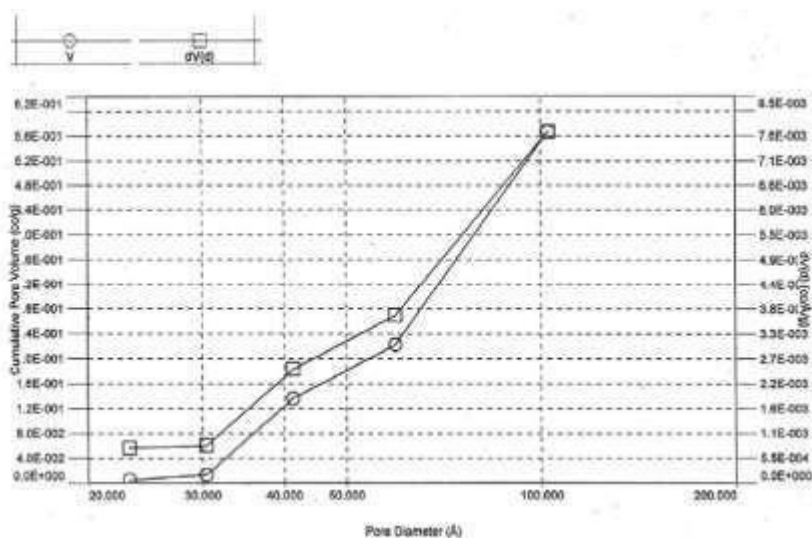
Figure 3.3. Graph showing distribution of pores in the prepared iron oxide iron oxide nanostructures from Water melon waste.

Table 3.12. Parameters (Physical) of the adsorbent synthesized from Water melonwaste

BET, Surface area (m^2/g)	71.35
Langmuir, Surface area (m^2/g)	261.50
Pore volume total (cm^3/g)	0.63
Micro Pores volume (cm^3/g)	0.27
Pore diameter, Average (A^0)	115.20

Table 3.12 displays the adsorbent's surface area analyzer data. According to the results, the Langmuir surface area was measured at 261.50 m2/g, while the BET surface area was determined to be 71.35 m2/g. The adsorbent made from watermelon waste had an average pore diameter of 115.20

A0, although the total and micropore volumes were found to be 0.63 cm3/g and 0.27 m3/g, respectively.
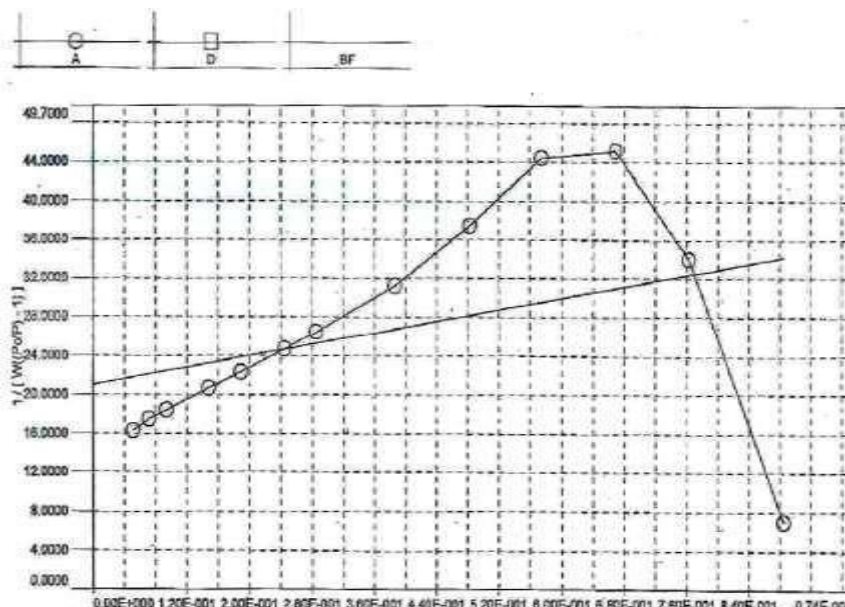
Figure 3.4. Graph showing BET surface area of the synthesized iron oxide ironoxide nanostructures from melon waste.
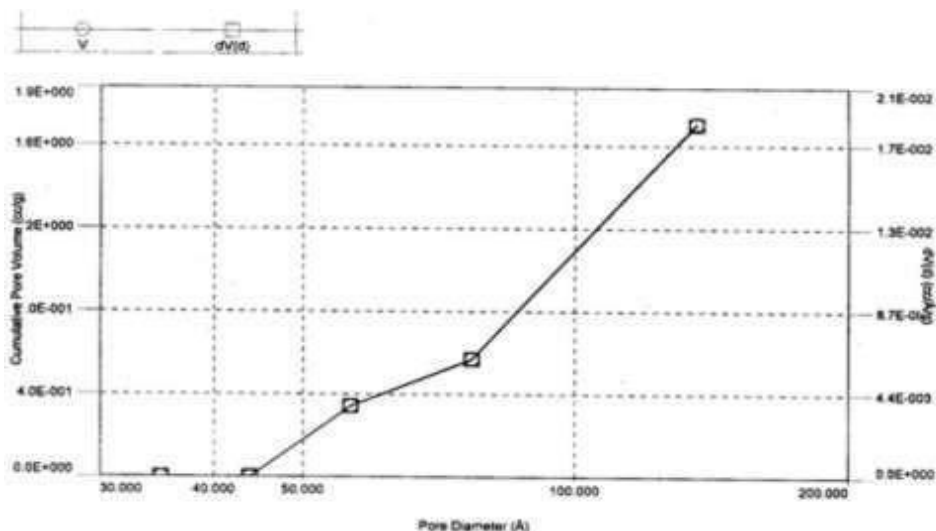
Figure 3.5. Graphical repsentation of pores distribution in the preparedadsorbent from melon waste

Table 3.13. Physical parameters of the adsorbent prepared from melon waste

BET, surface area (m^2/g)	100.77
Langmuir, surface area (m^2/g)	567.21
Pores volume, Total (cm^3/g)	2.07
Micro pores volume (cm^3/g)	0.81
Pore diameter, Average (A^0)	154.39
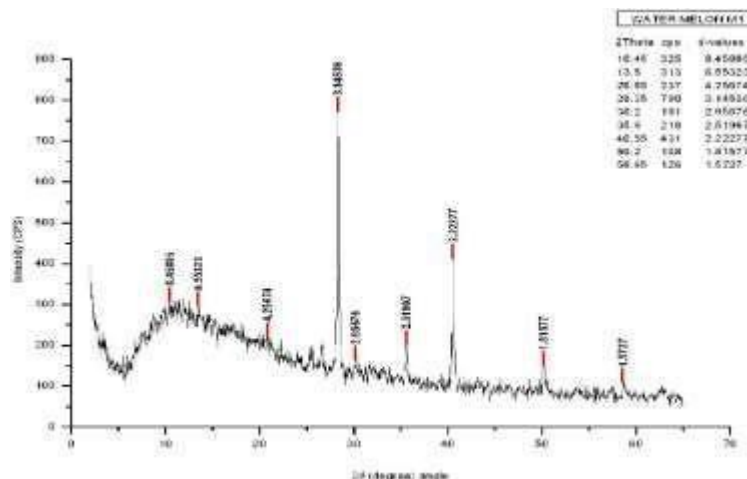
Table 3.13 displays the adsorbent's surface area analyzer data.

3.2.3 The produced adsorbents' characterization using an X-ray diffractometer (XRD)

Figure 3.6 shows the emphasized XRD spectra of the adsorbent made from watermelon waste, which indicates the presence of Fe3O4 deposited in carbon.

Figure 3.6. XRD spectra of iron oxide   nanostructures prepared from Watermelon waste
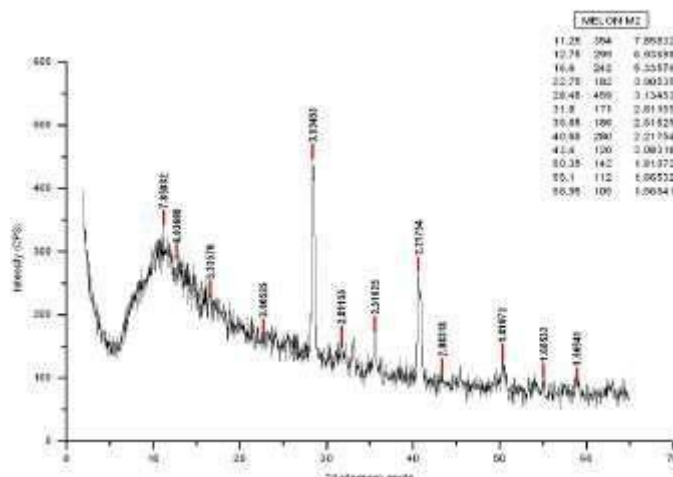
Figure 3.7. XRD pattern of iron oxide nanostructures prepared from melon waste

Iron oxide was found to be crystalline in the produced adsorbent made from melon waste, as shown by the XRD spectra (Figure 3.7). Iron oxide was also detected by the XRD patterns on the activated carbon.

The XRD method is utilized for both the particle size measurement and the structural analysis (Toth, 1995). The findings shown in Figure 3.6 demonstrated the existence of impurities in the form of Fe_2O_3 and Fe_3O_4. The matching indices to the diffraction peaks at 2θ are connected to the magnetite structure, as reported by (Robert & Mari, 2003; Dieter et al., 2005). According to Robert and Mari (2003), goethite (α FeO(OH), meghamite, and hematite are associated with the diffraction peaks at 2θ. According to Debye-Scherer's equation (4.1) the iron oxide particles were discovered to have sizes between 80 and 300 nm.

3.2.4 Infrared Spectroscopy Characterization of the Prepared Adsorbents

The most used method for characterizing nanostructures is infrared spectroscopy. The structural shape visible in the IR. Broad bands are indicative of iron oxide carbon nanostructures. Figures 3.8 and 3.9 depict the far and mid regions of the manufactured adsorbent's infrared spectrums. The adsorbent was made from watermelon waste and displayed a wide band at 1039.63 cm-1. According

to Wasserman et al. (2006) and Strachan (2010), the peaks at 1000–1200 cm-1 of the adsorbent indicate C–C and C–O stretching.
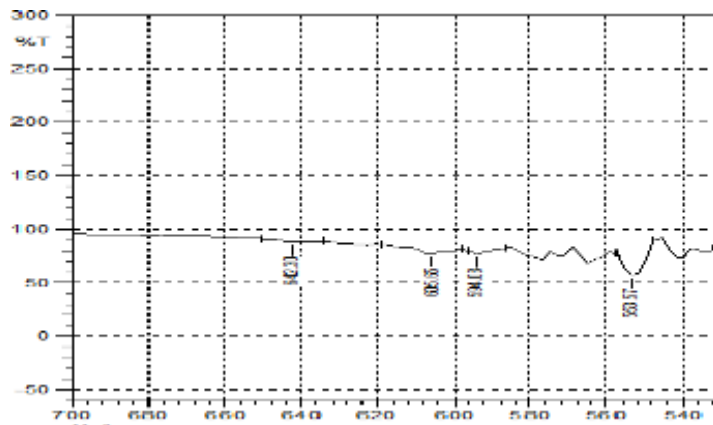
Figure 3.8: Far IR spectra of iron oxide nanostructures prepared from Watermelon waste
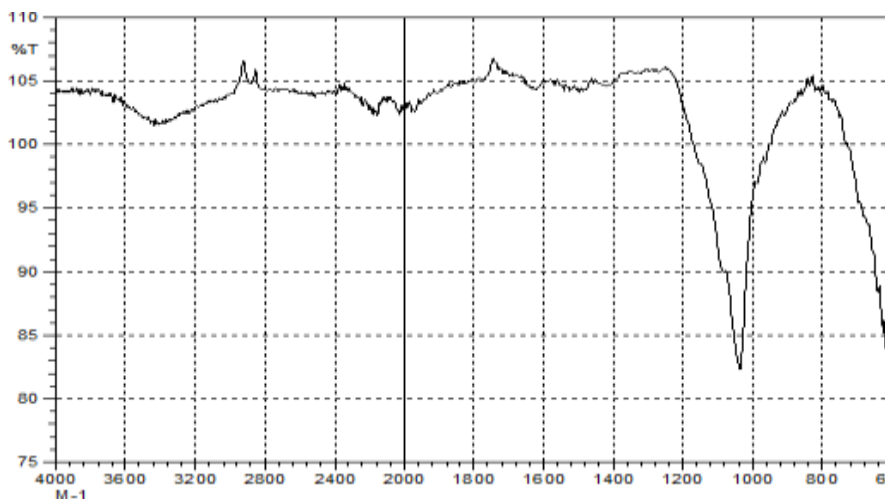
Figure 3.9: Mid IR spectra of iron oxide nanostructures prepared from Water melon waste.

The constructed adsorbent's IR spectra revealed a wide band peak, whereas the prepared adsorbent's FeO magnetite is responsible for stretching at 543.93.65 cm-1 (Groisman et al., 2004).
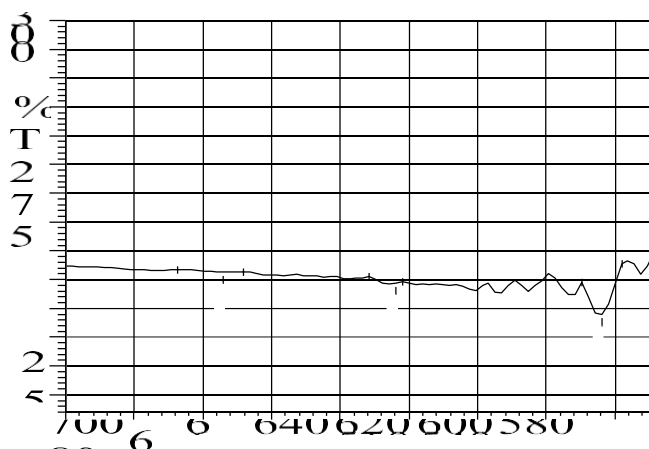
Figure 3.10: Far IR spectra of iron oxide nanostructures prepared from melon waste
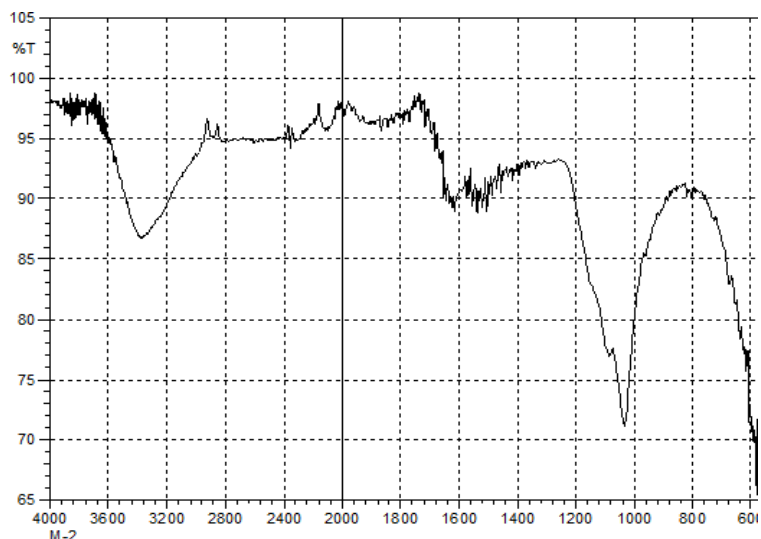
Figure 3.11: Mid IR spectra of iron oxide nanostructures prepared from melonwaste.

3.2.5. Adsorbents characterization by SEM

The surface morphology of the adsorbent made from watermelon waste is shown in Figure 3.12 at both high and low magnification. The produced composite's variations in size and form are shown by the SEM examination. The photos' white patches depict the manufactured iron oxide particles' crystalline structure, while the grayish regions indicate the presence of carbon. The pictogram showed how the moisture content absorbed by the prepared adsorbent causes iron oxide to aggregate. Nonetheless, it was discovered that the iron oxide carbon nanostructures ranged in size from 90 to 250 nm.
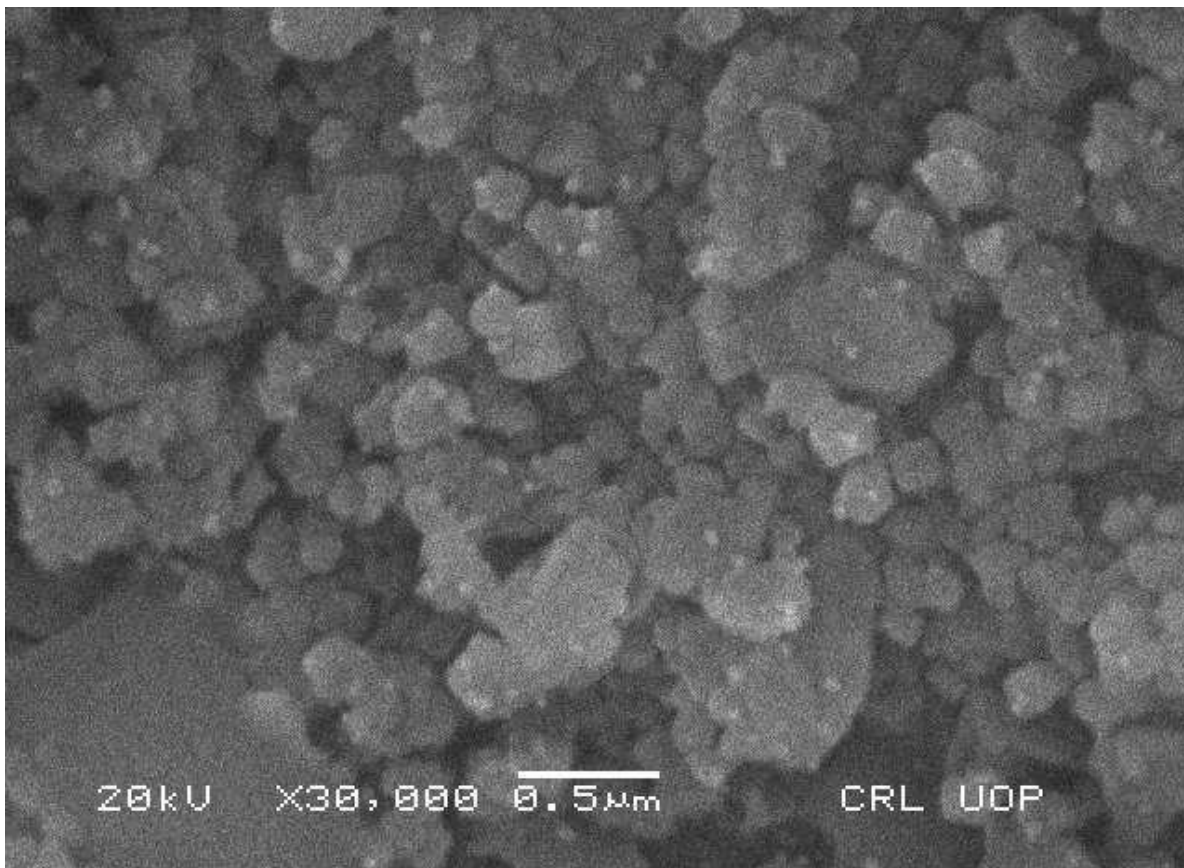
Figure 3.12. SEM pictures of water melon waste-derived iron oxide nanostructures at various magnifications

Figure 3.13 showing the iron oxide nanostructures' sizes and forms varied, as seen by the SEM. The crystalline iron oxide is shown by the white patches in the photos, while the black spots are associated with carbon. The agglomeration of iron oxide is ascribed to the moisture content that is absorbed by the produced adsorbent. The photos demonstrated that iron oxide had a spherical form and that nanostructures ranged in size from 70 to 300 nm.
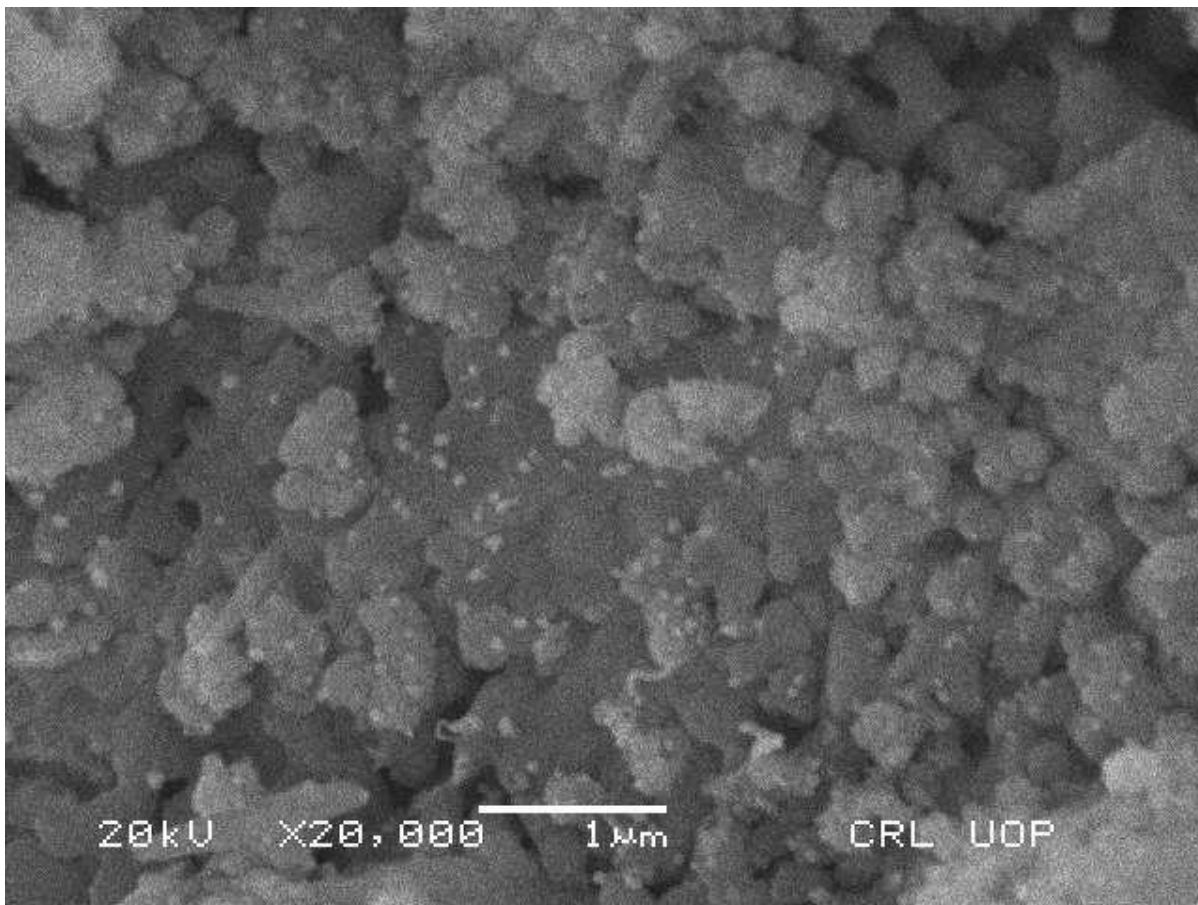
Figure 3.13: SEM pictures at various magnifications of iron oxide nanostructures made from melon waste

3.2.6 Using a differential thermal analyzer and thermogravimetric analyzer to characterise the produced adsorbents

Figure 3.14 shows that the spectra indicate two phases of dehydration; at 400–600 oC, there was an approximate 17.2% mass loss, while at 800-900 oC, there was a sudden 40% mass loss. At 970 oC, there was no discernible mass loss. Two endothermic peaks were discovered in the 300–500 °C range in the DTA study.
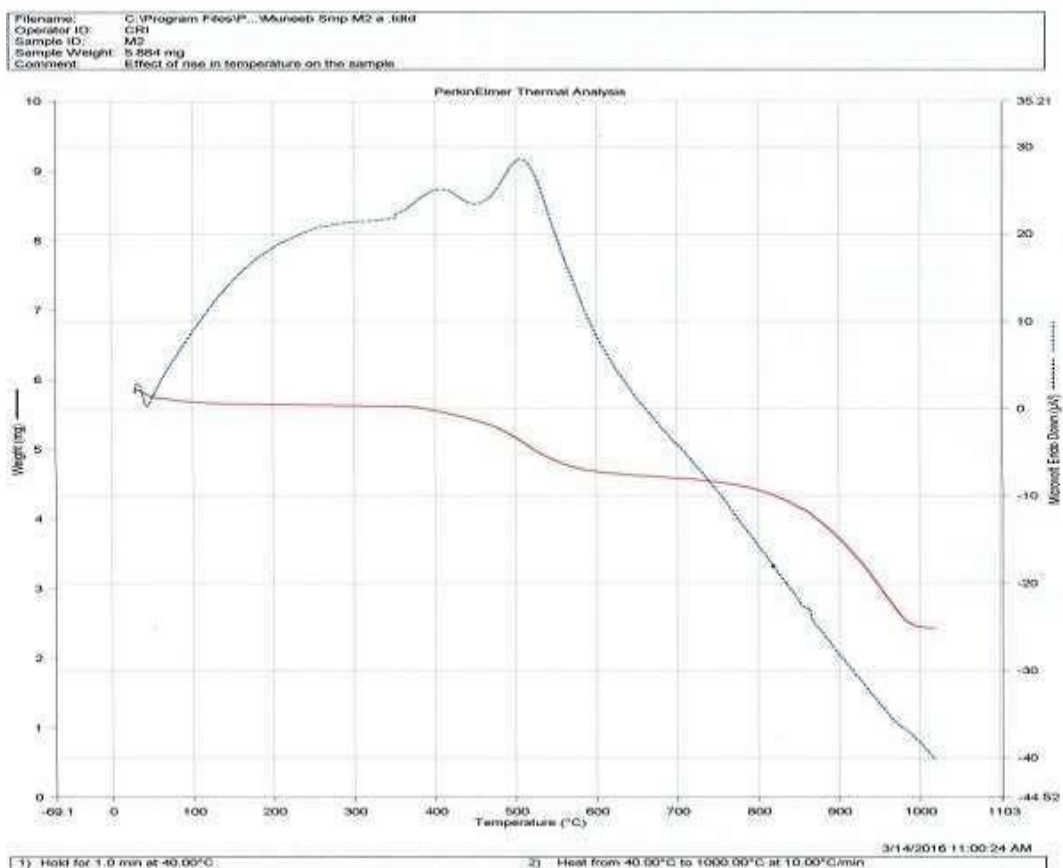
Figure 3.14: Iron oxide nanostructures' TG/DTA curves made from watermelon waste

The TG/DTA Spectra seen in Figure 3.15 are this. The result indicated two different periods of mass loss. Between 820 and 9800C, there was an additional mass loss of 45%, and between 4000 and 8200C, with an endothermic peak at 3800C, there was a mass loss of 7.54%.

Figure 3.15: Iron oxide nanostructures made from melon waste, using TG/DTA curves.

3.2.7 Electron Dispersive X-ray

Electron dispersive X-ray (EDX) technology is used to analyse the iron oxide nanostructures that are formed from watermelon waste, as seen in Figure 3.16. The findings show that carbon (C), iron (Fe), and oxygen (O) are present. There was a little Ca peak visible, indicating the impurity, according to Kahani et al. (2007), showed the deposition of iron oxide.
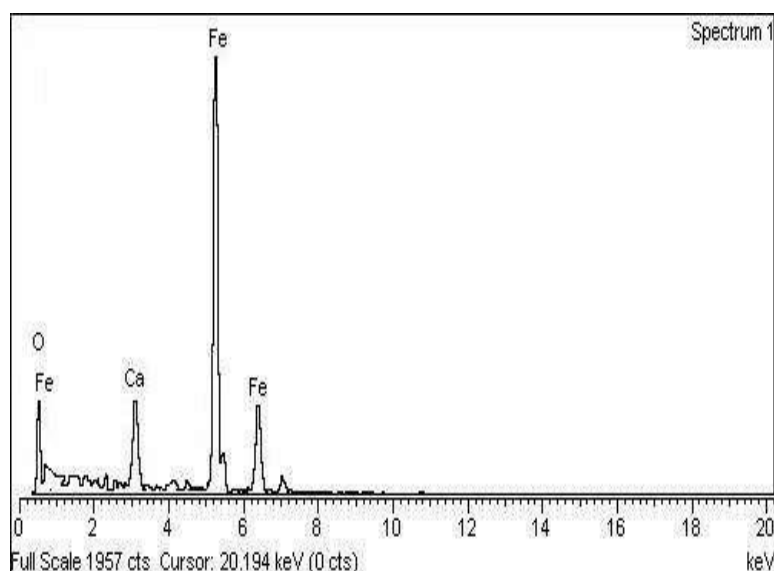
Figure 3.16: EDX spectra of water melon waste-prepared iron oxide nanostructures.

Figure 3.17 spectra revealed the presence of calcium as an impurity, whereas the presence of carbon, iron, and oxygen was indicated by a small peak, according Kahani et al. (2007).
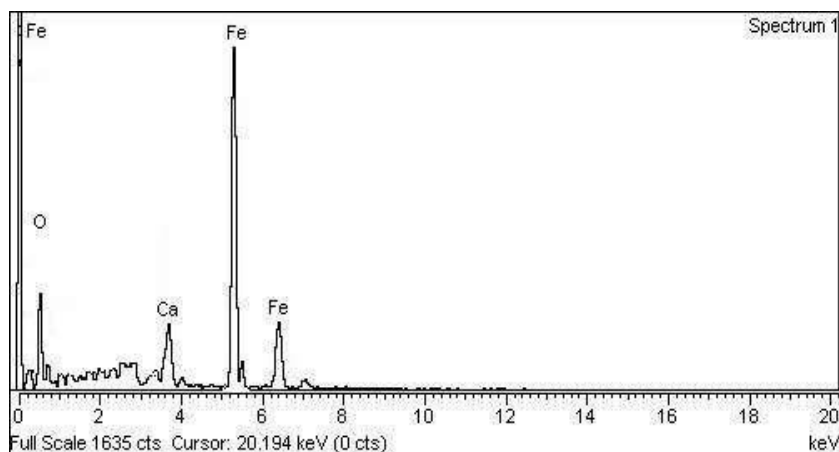
Figure 3.17: Iron oxide nanostructures made from melon waste and their EDX spectrum

3.3 Preparation of adsorbents for the removal of heavy metals
The following are the primary stages in the adsorption process that an adsorbent takes to remove an adsorbate:
● Transfer of entering particles to the adsorbent's outside surface.
● The adsorbate is transported through the adsorbent's pores, with the exception of a tiny amount of adsorption that takes place on the exterior surface.
● The most important step in this process is the rate-controlling step, which has an impact on the removal rate as a whole.

3.3.1 Isotherm of adsorption
Isotherms show that, up to saturation, the availability of adsorption sites was consistent for all concentrations. It may be explained by the continual partitioning of contaminants between the

substrate and solution up to the point of maximal adsorption. The linearity of the graphs makes it clear that there is a constant number of adsorption sites, and that as adsorption increases, more and more sites are produced. This is because the adsorbent is strongly attracted to the solute rather than the solvent.

3.3.1.1 The Langmuir isotherm
The Langmuir isotherm's linear form is as follows:

$$\frac{c}{q} = \frac{c}{Q_0} + \frac{1}{Q_0 b} \qquad (3.3)$$

In the equation above, q stands for the amount of adsorbate that has been adsorbed in milligrams. The equilibrium concentration of adsorbate in milligrams is denoted by g-1, C.L-1, where "Q0" and "b" are the Langmuir constants, "Q0" denotes the adsorbent's maximal adsorption capacity, and "b" denotes the process's energy.

Table 3.14: Langmuir adsorption constants for heavy metals adsorption on iron oxide nanostructures from watermelon and melon waste

Adsorbent	Heavy metals	Langmuir constant		R2
		Qo	B	
Watermelon waste	Arsenic	32894	0.025	0.929237
	Chromium	21012	0.021	0.9274
	Copper	38258	0.0078	0.8194
	Lead	29837	0.0312	0.8267
	Zinc	18654	0.0307	0.8192
Melon waste	Arsenic	19841	0.074	0.972411
	Chromium	18484	0.041	0.9014
	Copper	38285	0.0099	0.9431
	Lead	23752	0.0593	0.9386
	Zinc	26798	0.0231	0.8935

Figure 3.18 indicates equilibrium concentration against specific adsorption.
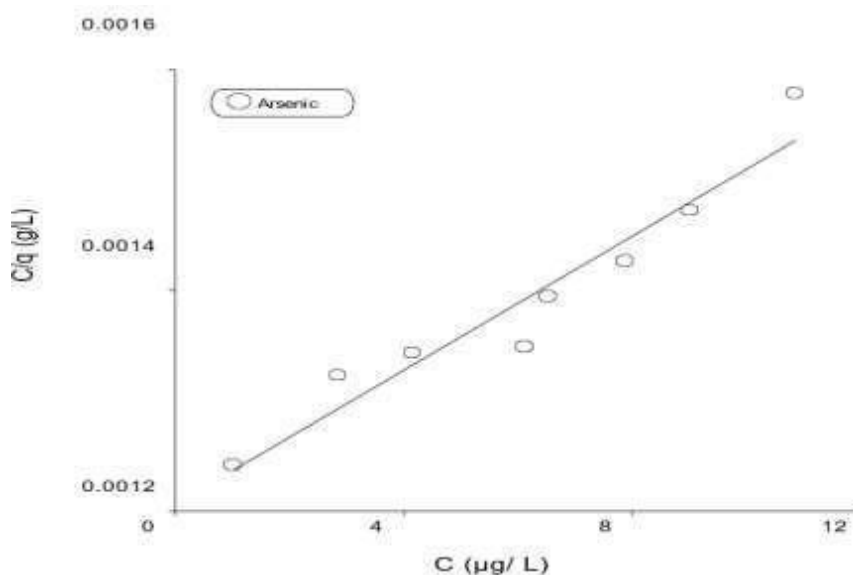
Figure 3.18: A Langmuir plot illustrated the arsenic adsorption on iron oxide nanoparticles synthesised from watermelon byproducts.

For an adsorbent manufactured from arsenic-containing melon byproduct, Figure 3.19.
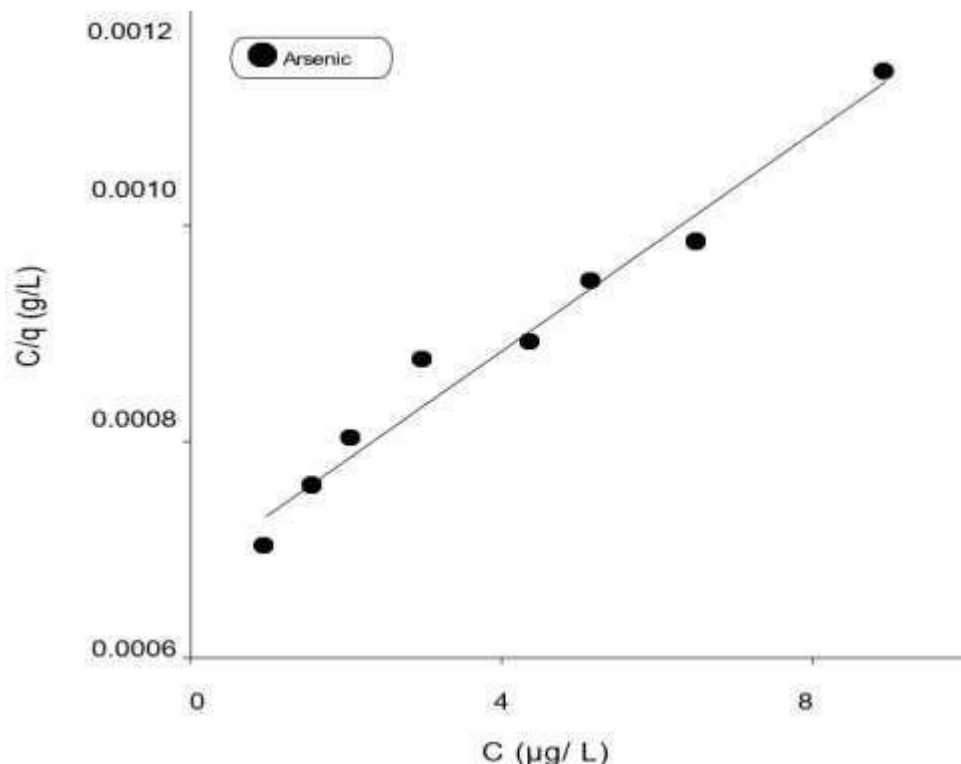
Figure 3.19: The Langmuir figure shows the rate of arsenic adsorption on iron oxide nanostructures made from melon byproducts.

Figure 3.20 show equilibrium concentration and specific adsorption relations for chromium.
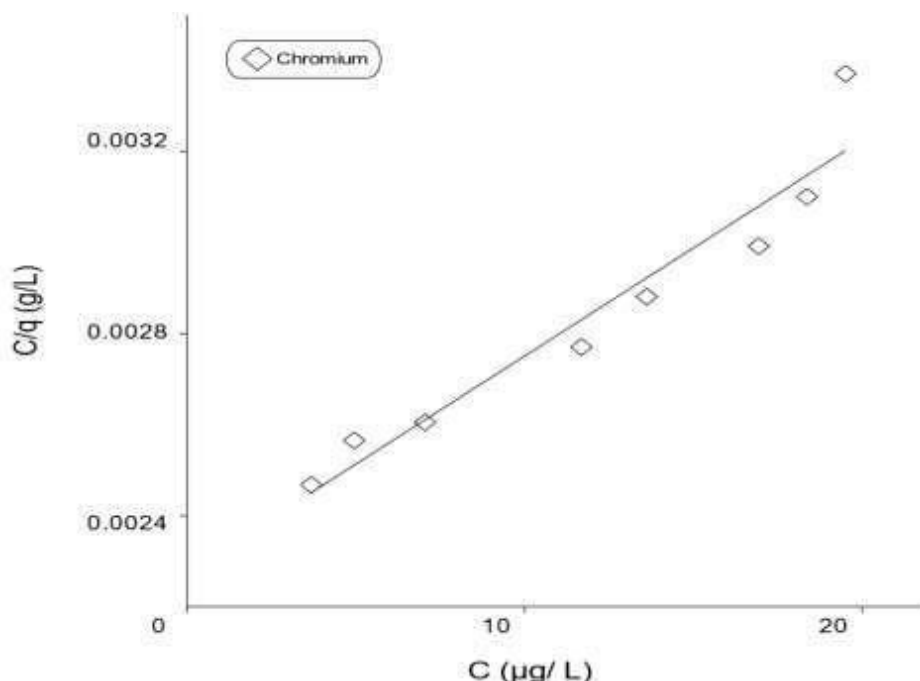
Figure 3.20: A Langmuir map demonstrates that iron oxide nanostructures synthesized from watermelon waste adsorb chromium.

The Langmuir Plot of specific adsorption (C/q) vs equilibrium concentration (C) for chromium is shown in Figure 3.21 for an adsorbent manufactured from melon waste. With an R2 value of 0.901

and a table value of 3.14, the Langmuir constants Q0 and b were calculated from the slope and intercept, resulting in values of 18484 and 0.041, respectively.
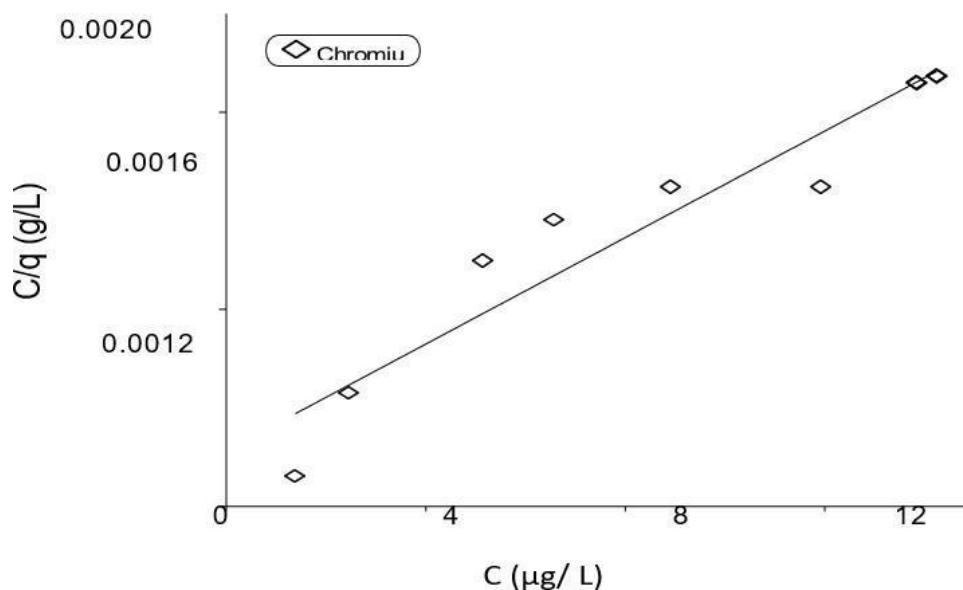
Figure 3.21: Nanostructures of iron oxide synthesized from discarded melon: a Langmuir plot for the adsorption of chromium.

Figure 3.22 show equilibrium concentration and specific adsorption relations for copper. Table 3.14 shows that the R2 value was 0.819, and the values of the Langmuir constants Q0 and b were 38258 and 0.0078, respectively, when the slope and intercept were used
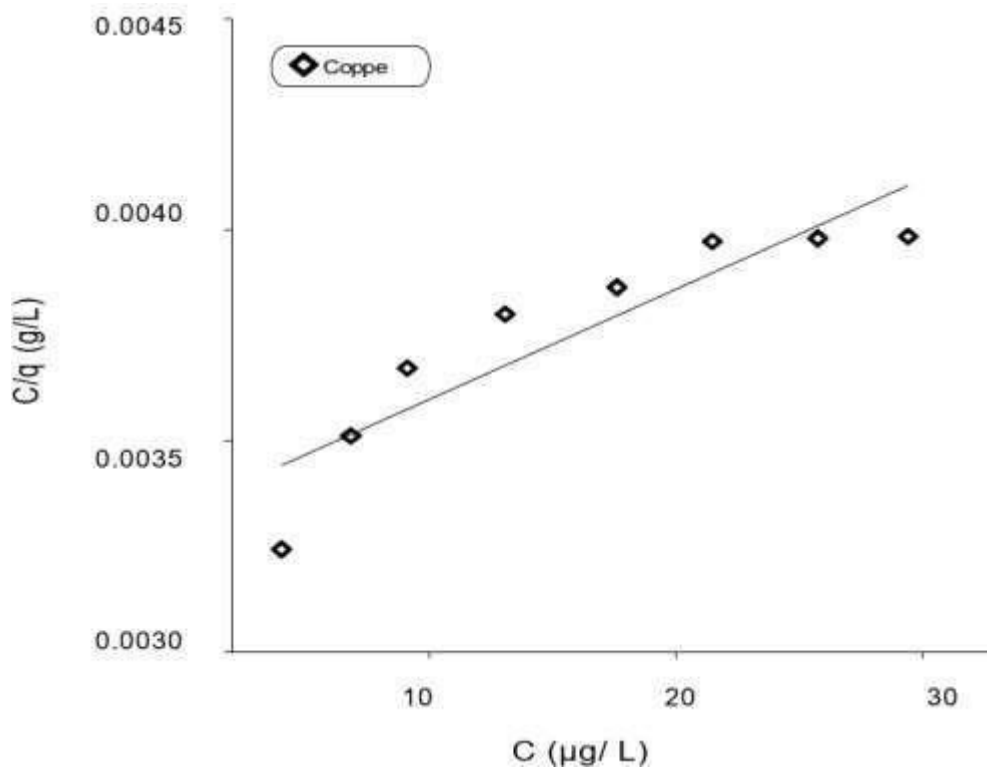
Figure 3.22: Langmuir plots reveal that iron oxide nanostructures synthesized from watermelon byproducts adsorb copper.

Figure 3.23 show equilibrium concentration and specific adsorption relations for copper made from melon waste. Table 3.14 shows that the R2 value was 0.9431, and the values of the Langmuir constants Q0 and b were 38285 and 0.0099, respectively, when the slope and intercept were used.
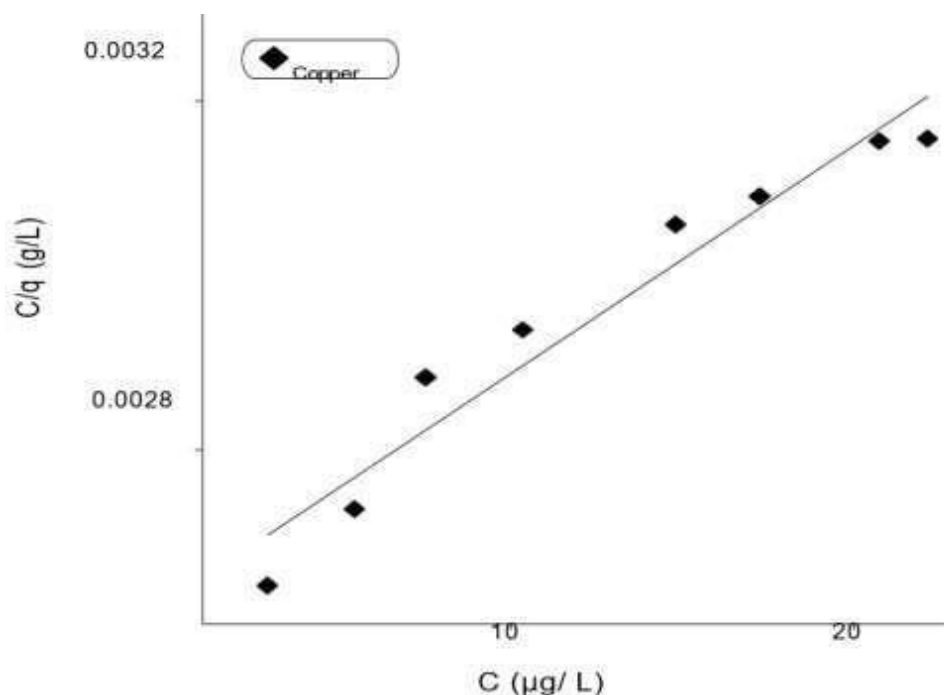
Figure 3.23: A Langmuir figure demonstrates the copper adsorption on iron oxide nanostructures synthesized from residual melon pulp.

Figure 3.24 show equilibrium concentration and specific adsorption relations for lead made from watermelon byproduct. We obtained a value of R2 0.826 from the slope and intercept, and the Langmuir constants Q0 and b were determined to be 29837 and 0.0312, respectively.
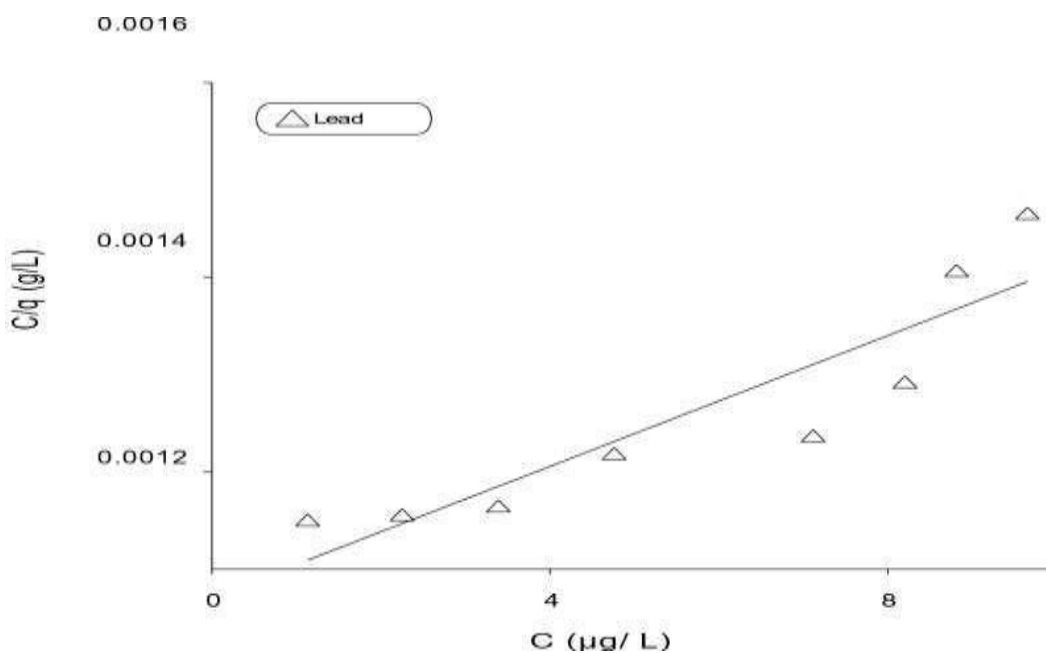
Figure 3.24: Langmuir plots reveal that iron oxide nanostructures synthesized from watermelon byproducts adsorb lead.

Figure 3.25 show equilibrium concentration and specific adsorption relations for lead made from melon waste. The slope and intercept were used to derive the Langmuir constants Q0 and b, which were 23752 and 0.059, respectively, with an R2 value of 0.938.
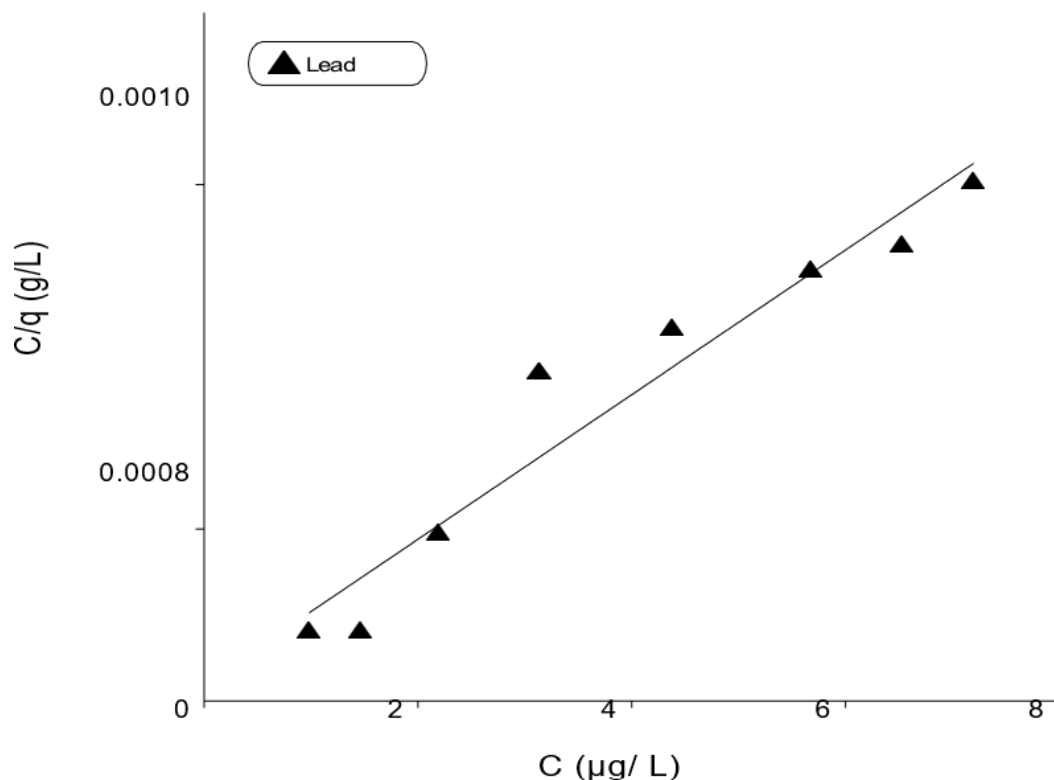
Figure 3.25: A Langmuir figure demonstrates the lead adsorption on iron oxide nanostructures synthesized from melon waste.

Figure 3.26 show equilibrium concentration and specific adsorption relations for zinc made from watermelon byproduct. From the slope and intercept, we may deduce that the Langmuir constants Q0 and b are 18654 and 0.0307, respectively, and that R2 is 0.819.
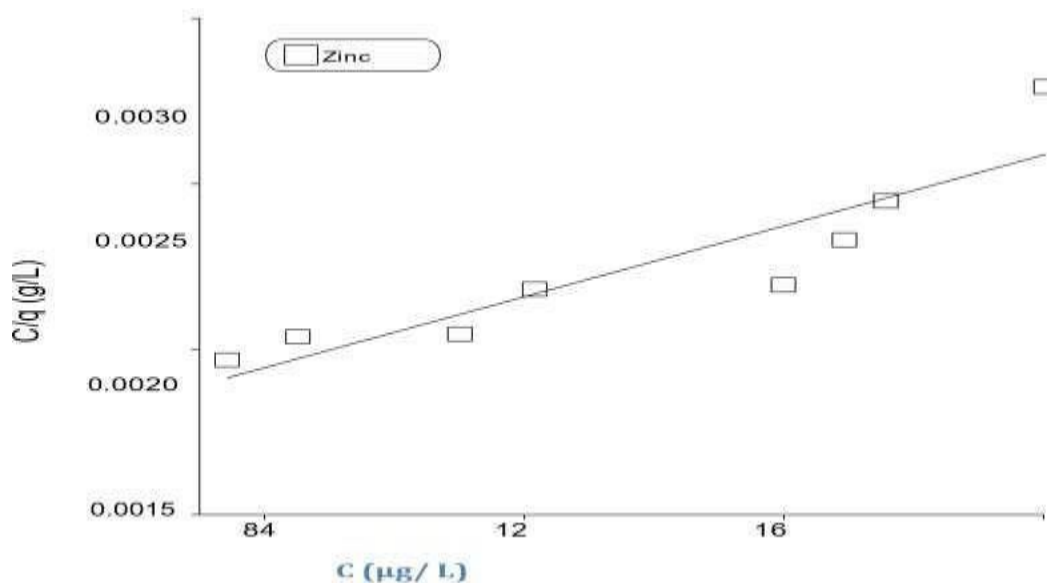
Figure 3 .26: Langmuir plots reveal that iron oxide nanostructures synthesized from watermelon byproducts adsorb zinc.

Figure 3.27 show equilibrium concentration and specific adsorption relations for lead made from melon waste. With an R2 value of 0.893, the slope and intercept were used to derive the Langmuir constants Q0 and b, which were 26798 and 0.0231, respectively.
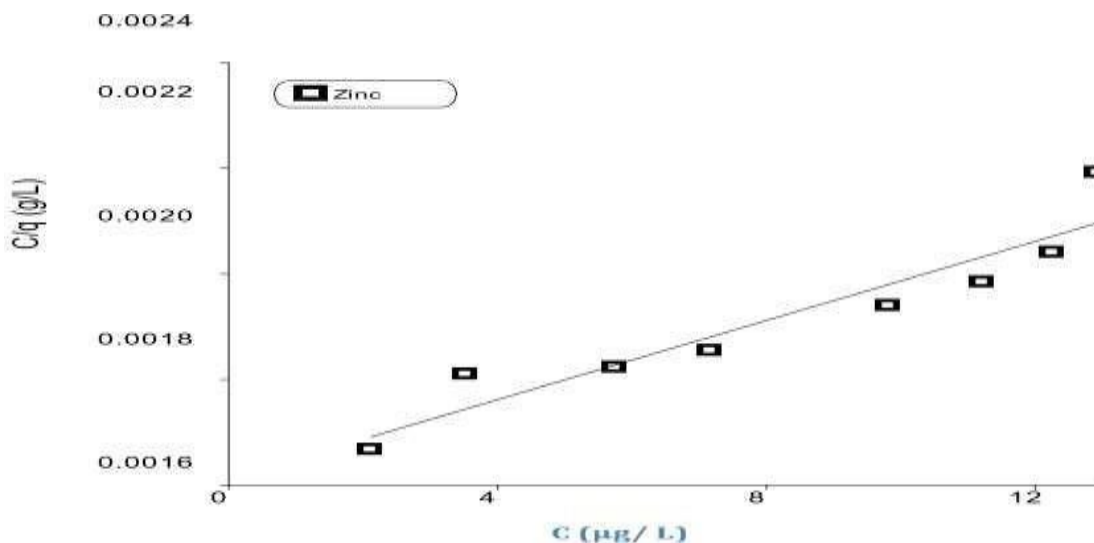
Figure 3.27**:** A Langmuir plot revealed that iron oxide nanostructures synthesized from residual cantaloupe waste adsorbed zinc.

3.3.1.2 Freundlich isotherm
This isotherm, which is provided by the equation, is mostly used to describe heterogeneous systems.

$$ln q = ln k + \frac{1}{n} ln C \quad (3.4)$$

The preceding equation uses K and n as Freundlich constants, C to represent the equilibrium concentration in milligrams L-1, and q to represent the quantity of adsorbate adsorbed in milligrams per gram. While n denotes the adsorption intensity, K is the adsorption capacity. The slope and intercept of the lnC versus lnq plot may be used to get the Freundlich constants K and 1/n.

Table **3.15.** Freundlich constants for adsorption of heavy metals on iron oxide nanostructures prepared from watermelon waste and melon waste.

Adsorbent	Heavy metals	Freundlich constant		R2
		1/n	K	
Watermelonwaste	Arsenic	0.9040	859.25	0.9810
	Chromium	1.0944	277.86	0.9617
	Copper	1.004	261.25	0.9834
	Lead	0.9156	905.87	0.9910
	Zinc	1.1910	292.96	0.9709
Melonwaste	Arsenic	0.9257	1231.82	0.95194
	Chromium	0.8192	806.722	09867
	Copper	0.9784	356.49	0.9915
	Lead	0.9568	1203.40	0.9694
	Zinc	1.0752	452.73	0.9907

In Figure 3.28, we can see the Freundlich adsorption of arsenic on an adsorbent manufactured from watermelon pulp. With an R2 value of 0.981, the iron oxide nanostructures synthesized from watermelon waste had K and l/n values of 859.25 and 0.904, respectively.
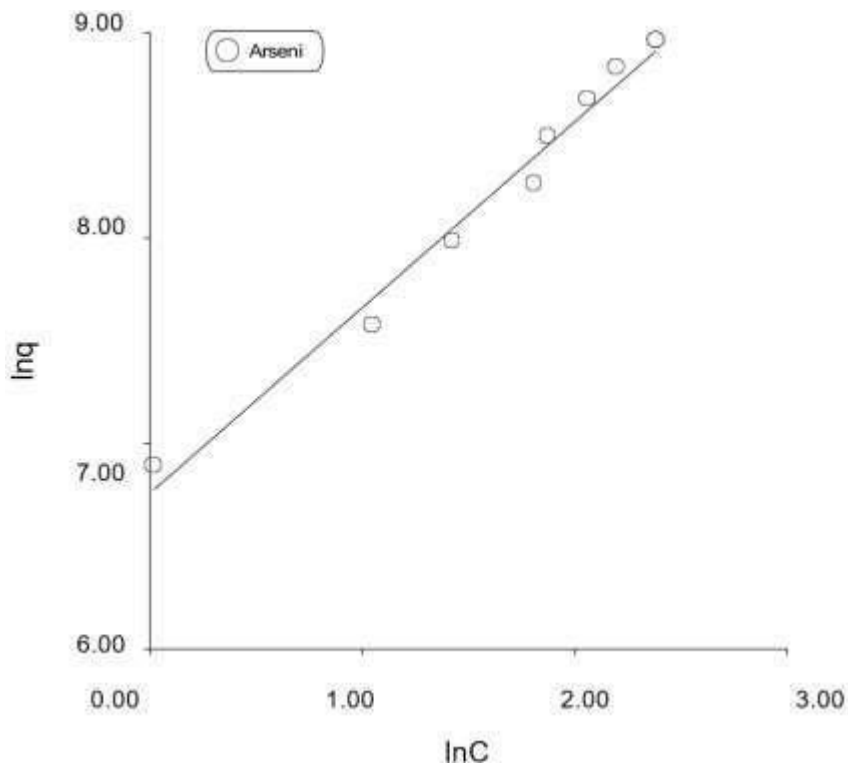
Figure 3.28: Arsenic adsorption Freundlich plot on iron oxide nanostructures made from watermelon byproducts.

In Figure 3.29, we can see the Freundlich adsorption of arsenic on iron oxide nanostructures synthesized from melon byproducts. With an R2 value of 0.951 and K and 1/n values estimated from the plot of 1231.82 and 0.926, respectively, the iron oxide nanostructures generated from melon waste were listed in Table 3.15.
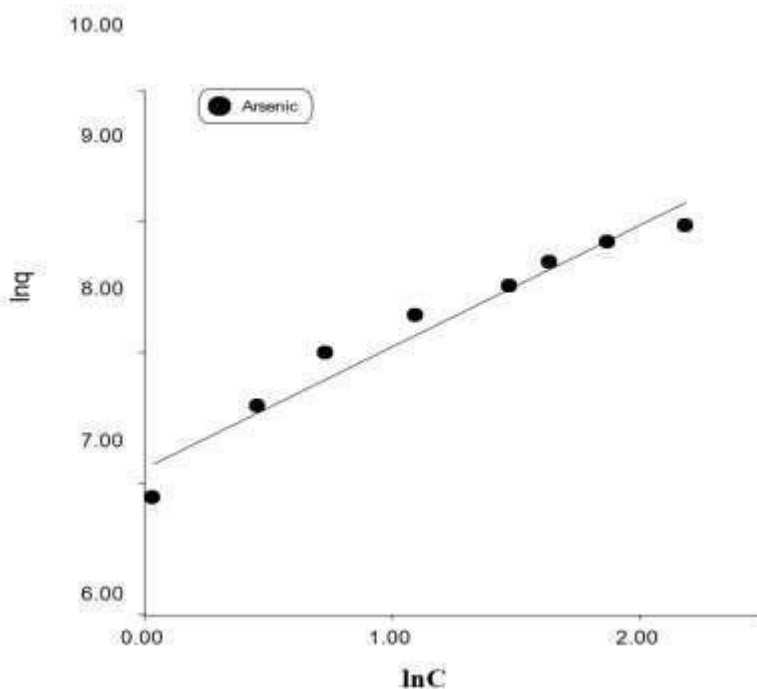
Figure 3.29: Arsenic adsorption on iron oxide nanostructures synthesized from cantaloupe byproducts, as seen in a Freundlich plot.

As demonstrated in Figure 3.30, the adsorbent manufactured from watermelon waste exhibited Freundlich adsorption for chromium. Figure 4.40 shows that the nanostructures produced from watermelon byproducts had a K value of 277.86 and a 1/n value of 1.094, while Table 3.15 shows that the R2 value was 0.961
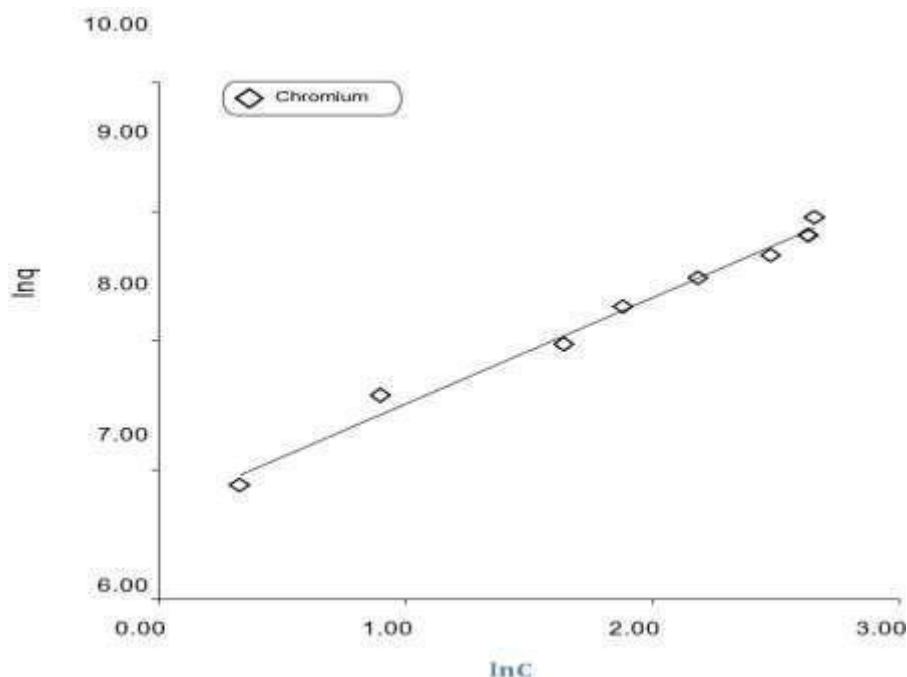
Figure 3.30: Iron oxide nanostructures synthesized from watermelon byproducts exhibit chromium adsorption, as shown in a Freundlich plot.

Figure 3.31 shows the Freundlich adsorption of chromium onto an adsorbent manufactured from discarded melons. Figure 3.31 shows that the nanostructures produced from melon waste had a K value of 806.72 and a 1/n value of 0.819. Table 3.15 shows that the R2 value was 0.998.
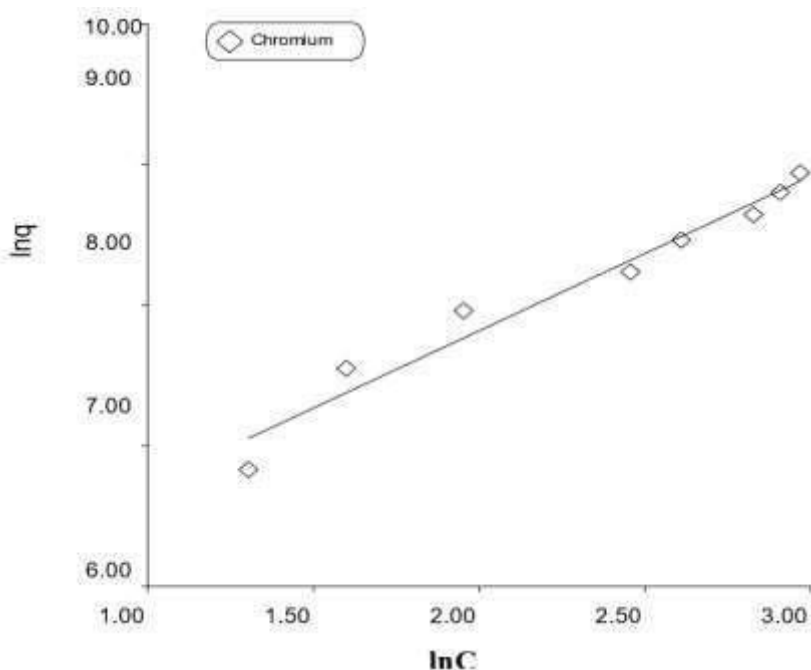
Figure 3 .31: Adsorption of chromium onto iron oxide nanostructures synthesized from cantaloupe byproducts: a Freundlich plot.

Figure 3.32 displays the Freundlich adsorption for copper adsorption on an adsorbent manufactured from watermelon waste. Figure 3.32 shows that the nanostructures produced from watermelon byproducts had a K value of 261.25 and a 1/n value of 1.004. Table 3.15 shows that the R2 value was 0.983.
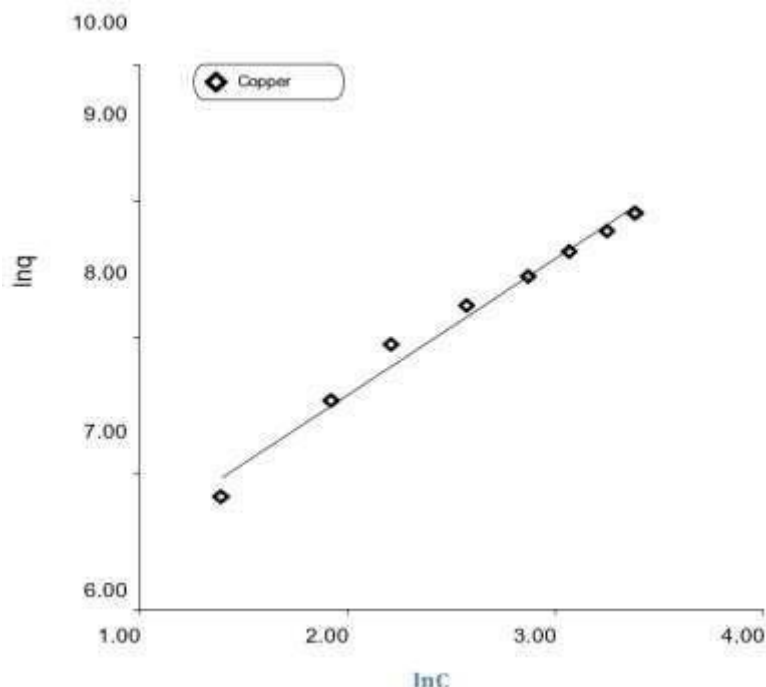
Figure 3 .32: The Freundlich plot was used to study the copper adsorption on iron oxide nanostructures that were synthesized from watermelon waste.

Figure 3.33 shows the Freundlich adsorption of copper on an adsorbent manufactured from melon waste. Figure 3.33 shows that the nanostructures produced from melon waste had a K value of 56.49 and a 1/n value of 0.978. Table 3.15 shows that the R2 value was 0.991.
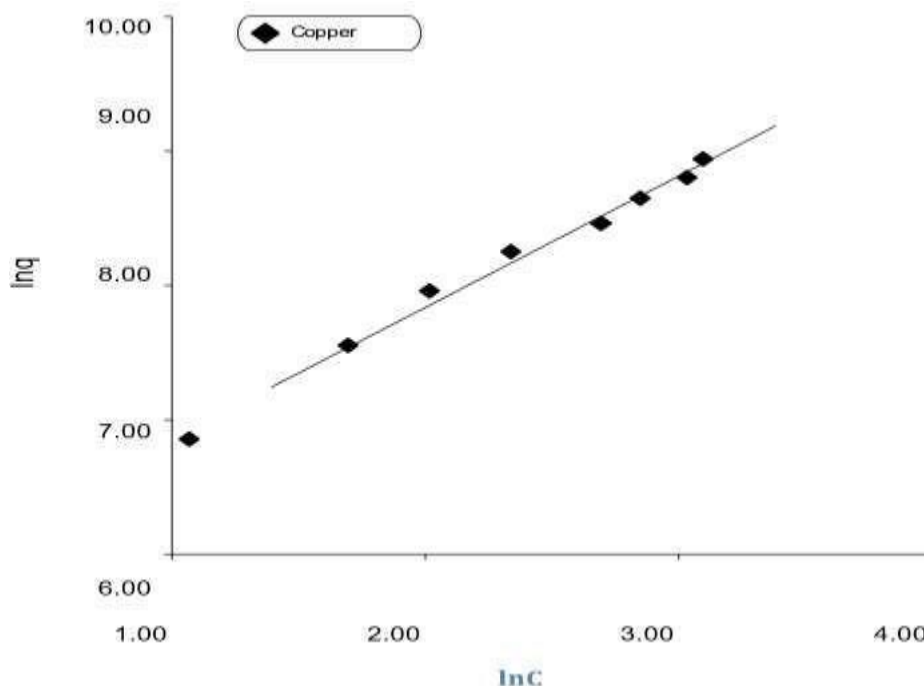
Figure 3 .33: A Freundlich plot illustrating the adsorption of copper onto iron oxide nanostructures synthesized from discarded melon segments is shown.

Figure 3.34 shows the Freundlich adsorption of lead onto an adsorbent manufactured from watermelon byproducts. Table 3.15 shows an R2 value of 0.991 and K and 1/n values of 905.87 and 0.915, respectively, for nanostructures produced from watermelon waste (Fig. 3.34).
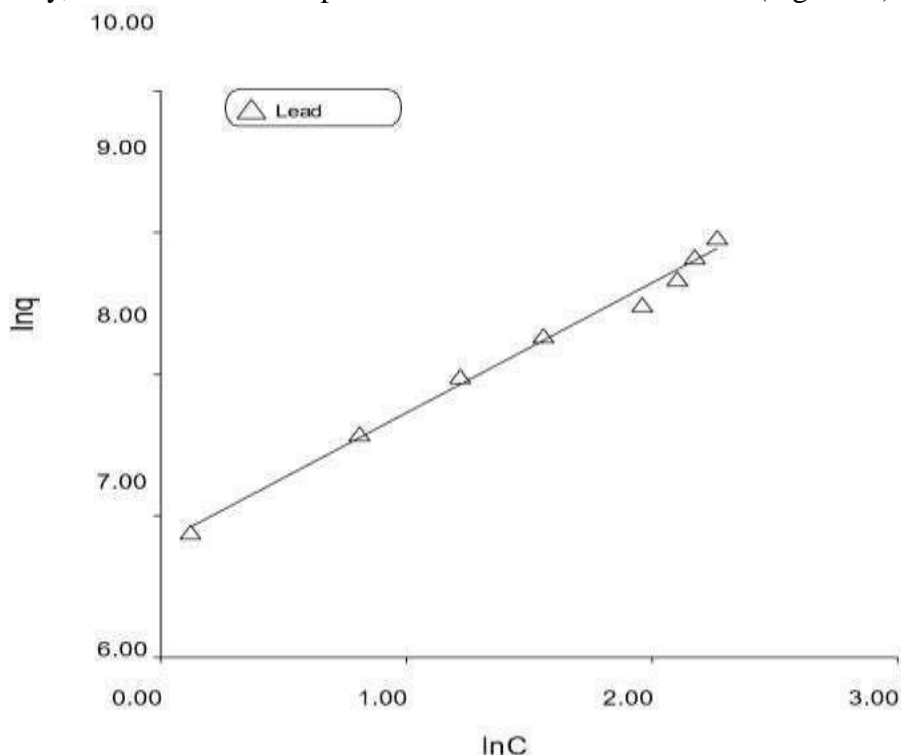
Figure 3.34: The Freundlich plot was used to study the lead adsorption process on iron oxide nanostructures synthesized from watermelon pits.

Figure 3.35 shows the Freundlich adsorption of lead onto an adsorbent manufactured from discarded melons. Table 3.35 shows an R2 value of 0.969 and K and 1/n values of 1203.40 and 0.957, respectively, for nanostructures produced from melon waste (Fig. 3.35).
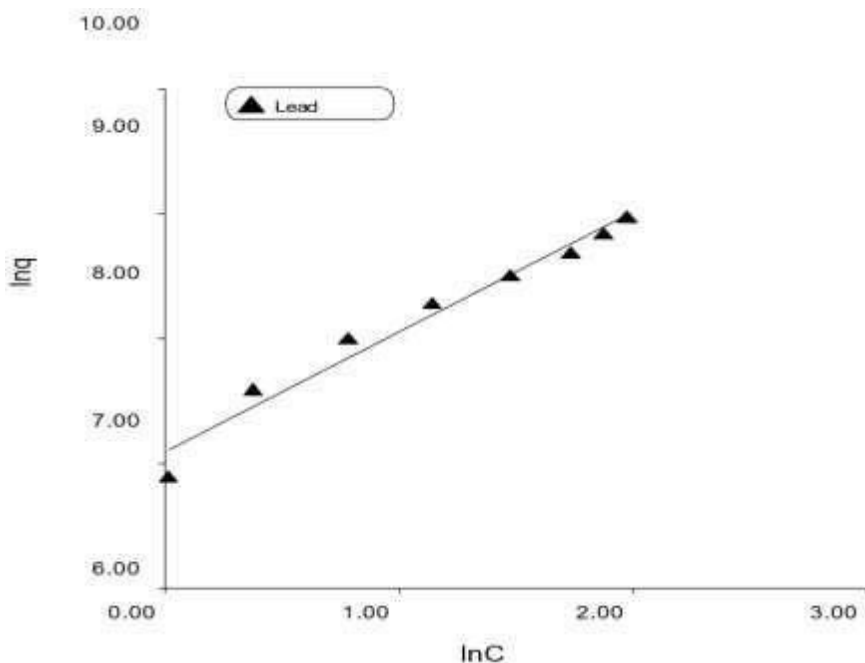
Figure 3 .35: A Freundlich plot illustrating the lead adsorption process on iron oxide nanoparticles synthesized from cantaloupe byproducts.

Figure 3.36 displays the Freundlich adsorption relationship between a watermelon waste adsorbent and zinc. Figure 3.36 shows that the nanostructures produced from watermelon byproducts had a K value of 292.96 and a 1/n value of 1.191, while Table 3.15 shows that the R^2 value was 0.971.
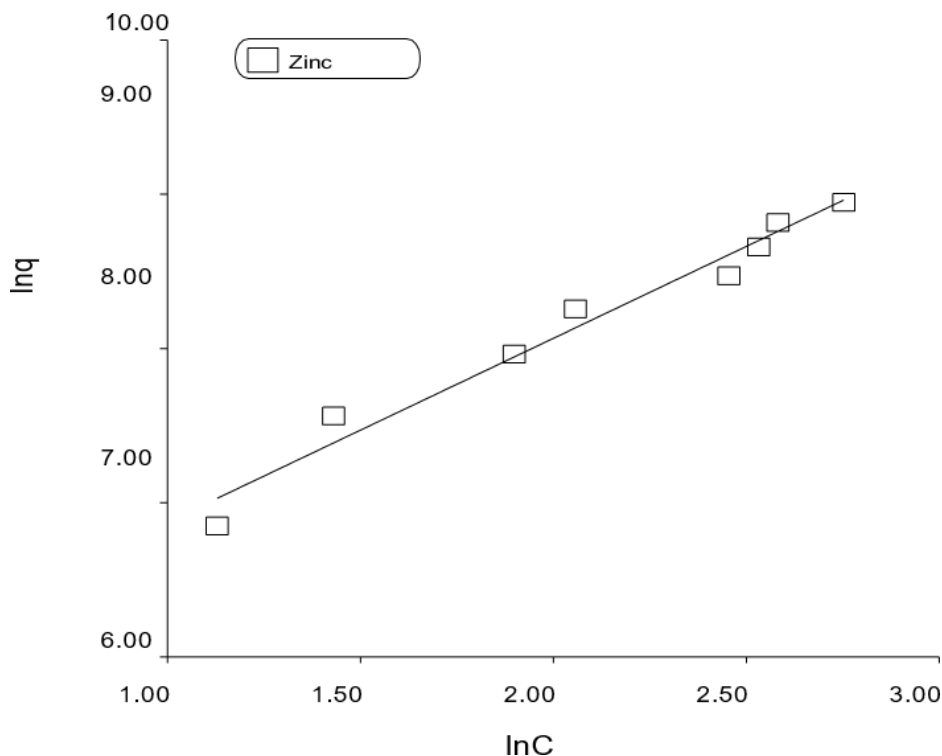
Figure 3 .36: The Freundlich plot approach was used to study the zinc adsorption on iron oxide nanostructures that were synthesised from watermelon waste.

As demonstrated in Figure 3.37, adsorbents manufactured from melon waste exhibit Freundlich adsorption for zinc. The K and 1/n values for the melon waste nanostructures were 452.73 and 1.075, respectively, according to Fig. 3.37. The R^2 value was 0.991, as shown in Table 3.15.
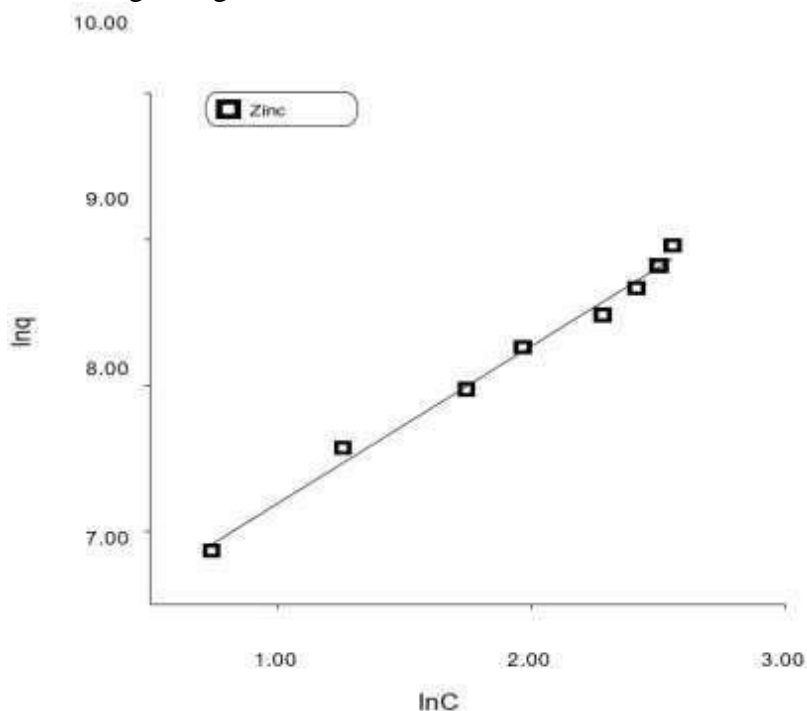
Figure 3.37: The Freundlich plot displays the adsorption of zinc onto iron oxide nanoparticles synthesised from cantaloupe byproducts.

In contrast to the Langmuir isotherm, the Freundlich adsorption isotherm showed that the data were more matched to the adsorbents' data. Table 3.15, as shown by the higher R2 values that were achieved.

3.4 Adsorption kinetics
3.4.1 Effect of contact time:

The amount of contact time an adsorbent needs to attain equilibrium is a crucial component in adsorption operations. The equilibrium contact time for arsenic is shown in Figures 3.39 and 3.40. Since there were originally more adsorbent sites accessible for the adsorption of metal, the absorption of arsenic occurred relatively quickly in the first few minutes. Slow adsorption occurs as a result of the metals occupying the greatest number of sites over time. The adsorbents' saturation causes the equilibrium time of adsorption to occur at the conclusion. The equilibrium times for the adsorbent made from watermelon and melon waste are 260 minutes and 240 minutes, respectively, as Figures 3.39 and 3.50 illustrate.
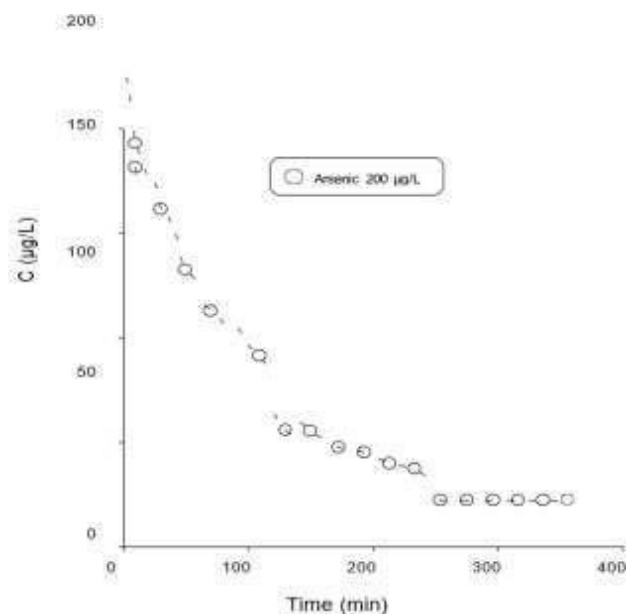
Figure 3.38: The impact of contact duration on the arsenic adsorption process on iron oxide nanostructures synthesised from watermelon byproducts is shown.
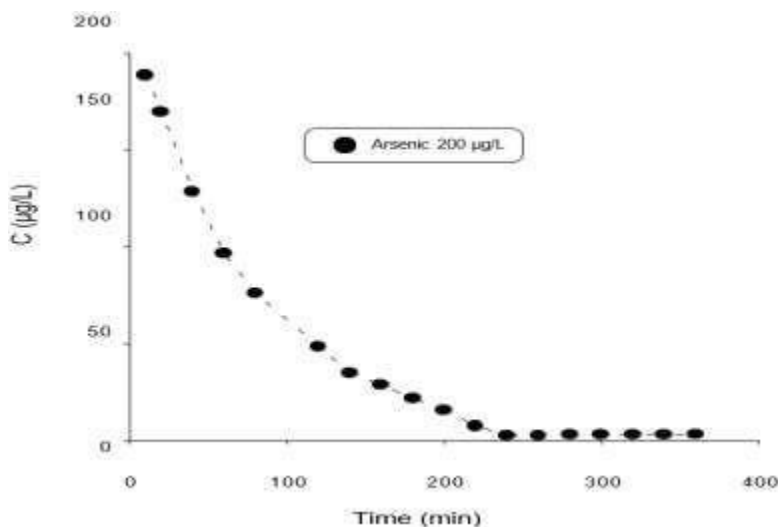
Figure 3.39: Arsenic adsorption on iron oxide nanostructures synthesised from cantaloupe byproducts as a function of contact time, as shown in graphic form.

Figures 3.40 and 3.41 show the contact time for chromium needed to attain equilibrium. The absorption of chromium occurred in a matter of minutes, as there were originally more adsorbent sites accessible for the adsorption of metal. As time goes on, the metals occupy the greatest number of sites, which causes the adsorption process to proceed slowly. The adsorbents' saturation causes the equilibrium time of adsorption to occur at the conclusion. Iron oxide nanostructures made from watermelon and melon waste had an equilibrium duration of 220 minutes and 260 minutes, respectively, as Figures 3.40 and 3.41 demonstrate.
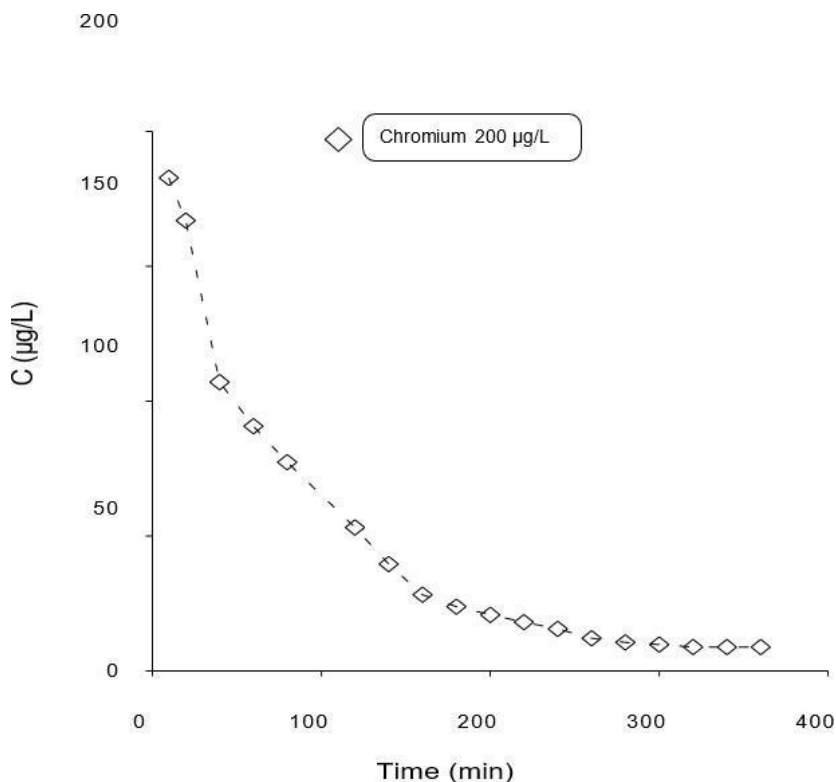
Figure 3.40: Iron oxide nanostructures synthesised from watermelon byproducts demonstrate the impact of contact duration on chromium adsorption.
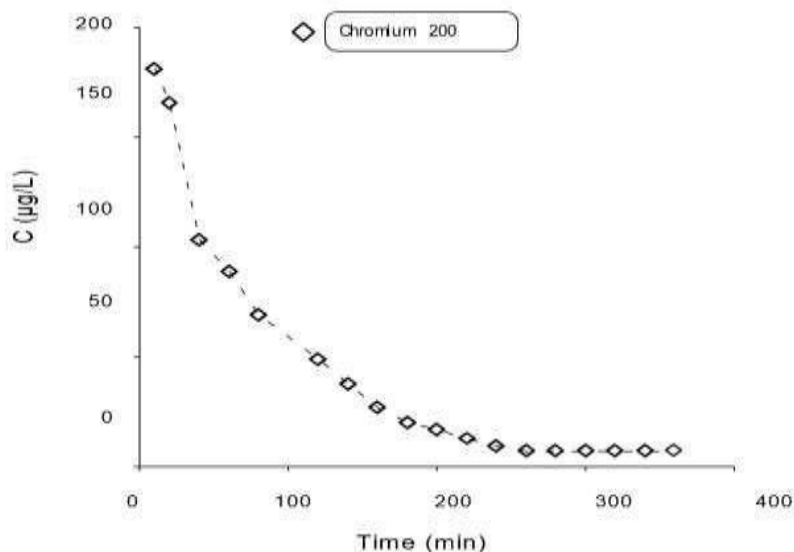
Figure 3.41: The interaction between contact time and discarded melon nanostructures for chromium adsorption is seen in the picture.
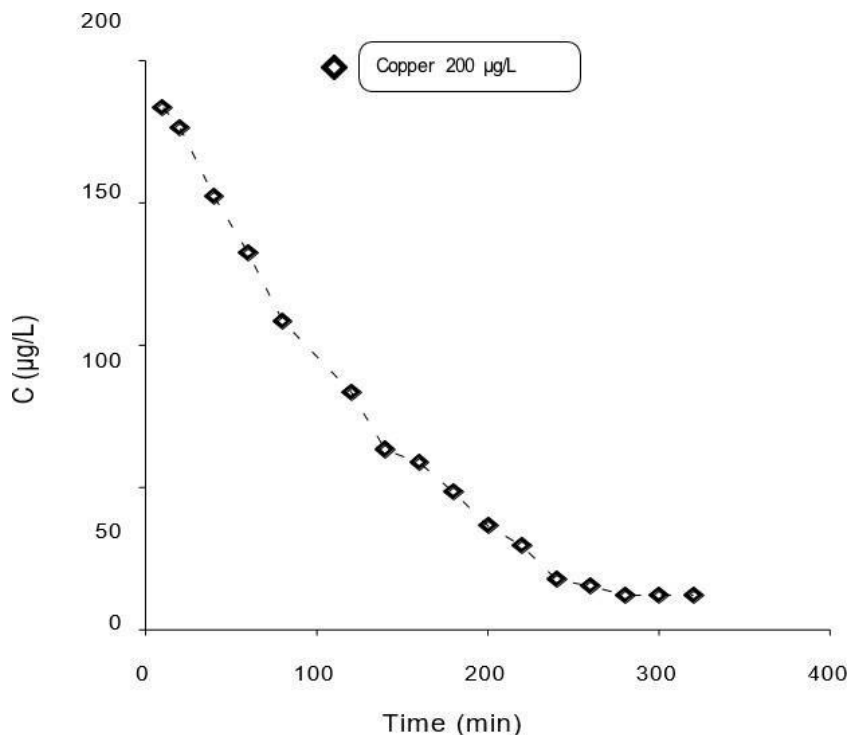
Figure 3.42: Iron oxide nanostructures synthesised from watermelon byproducts demonstrate the impact of contact duration on copper adsorption.

In Figures 3.42 and 3.43, the contact time for copper needed to attain equilibrium is shown. Since there were originally more adsorbent sites accessible for the adsorption of metal, the absorption of copper happened relatively quickly in the first few minutes. The metal occupies a maximum number of sites over time, which causes the adsorption process to proceed slowly. The adsorbents' saturation causes the equilibrium time of adsorption to occur at the conclusion. The equilibrium times for adsorbent prepared watermelon and melon trash are 280 minutes and 240 minutes, respectively, as Figures 3.42 and 3.43 demonstrate.
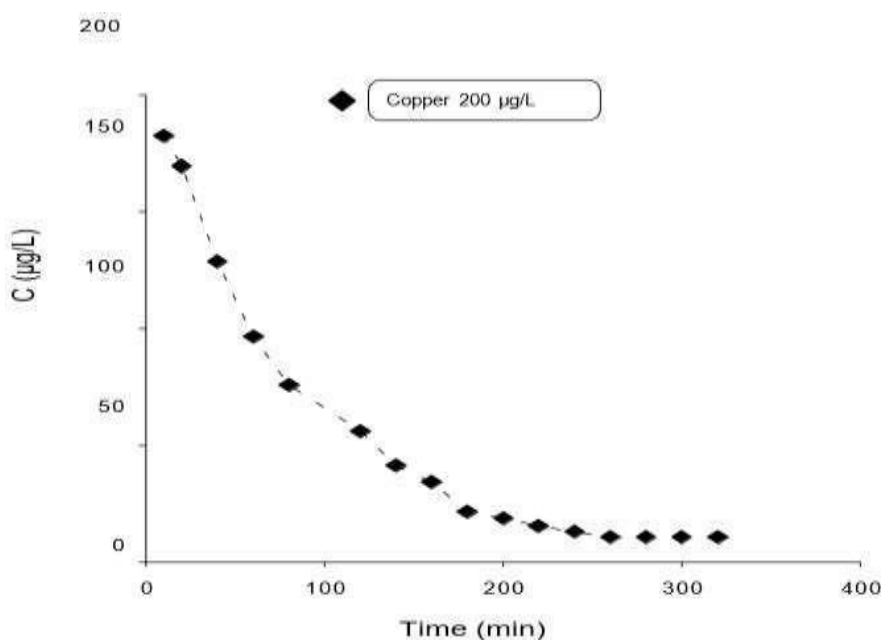
Figure 3.43: Demonstrate that iron oxide nanostructures generated from residual melon waste affect copper adsorption as a function of contact time.

Since there were originally more adsorbent sites accessible for the adsorption of metal, the absorption of lead occurred quite quickly in the first few minutes. The adsorption process slows down as time goes on because the metals occupy the greatest number of sites. The adsorbents' saturation causes the equilibrium time of adsorption to occur at the conclusion. The equilibrium times for the adsorbent made from watermelon and melon waste are 200 and 220 minutes, respectively, as Figures 3.44 and 3.45 illustrate.
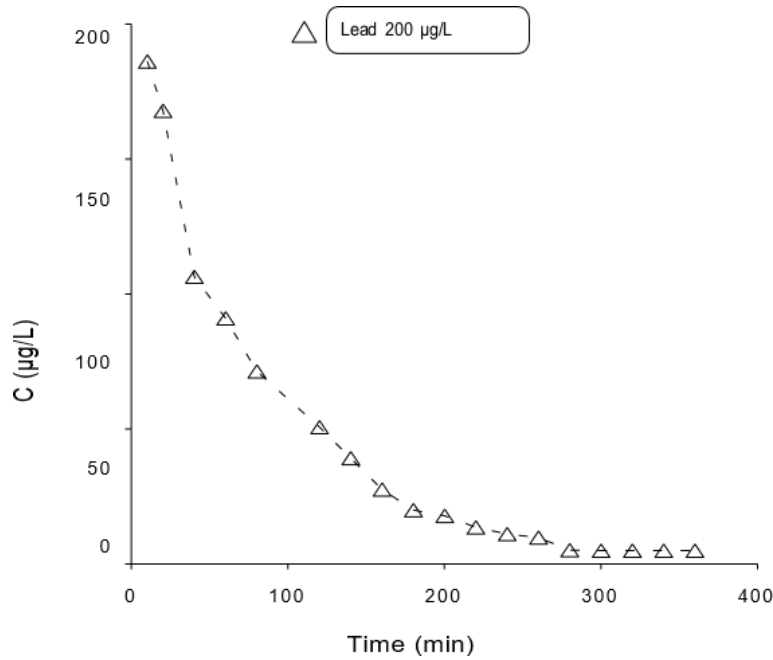
Figure 3.44: It is shown that the lead adsorption on iron oxide nanostructures synthesised from watermelon byproducts is affected by the contact time.
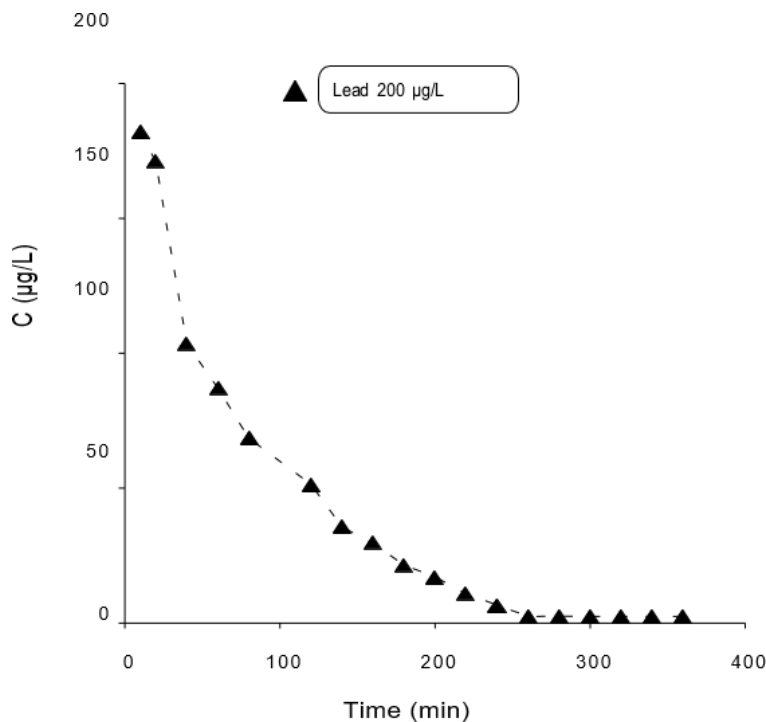
Figure 3.45: The graph illustrates the relationship between contact time and lead adsorption on nanostructures made of discarded melon.

In Figures 3.46 and 3.47, the contact time for zinc needed to attain equilibrium is shown. Since there were originally more adsorbent sites accessible for the adsorption of metal, the absorption of zinc happened relatively quickly in the first few minutes. Slow adsorption occurs as a result of the metals occupying the greatest number of sites over time. The adsorbents' saturation causes the equilibrium time of adsorption to occur at the conclusion. The equilibrium times for adsorbent made from watermelon and melon waste are 200 and 180 minutes, respectively, as Figures 3.46 and 3.47 illustrate.
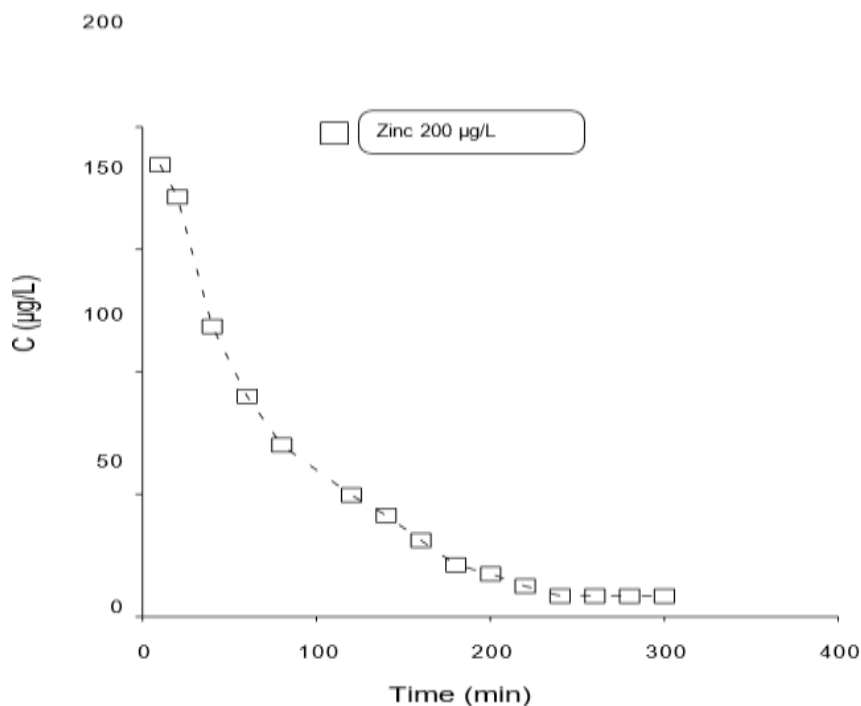
Figure 3 .46: Iron oxide nanostructures synthesised from watermelon byproducts and the effect of contact duration on zinc adsorption are shown graphically.
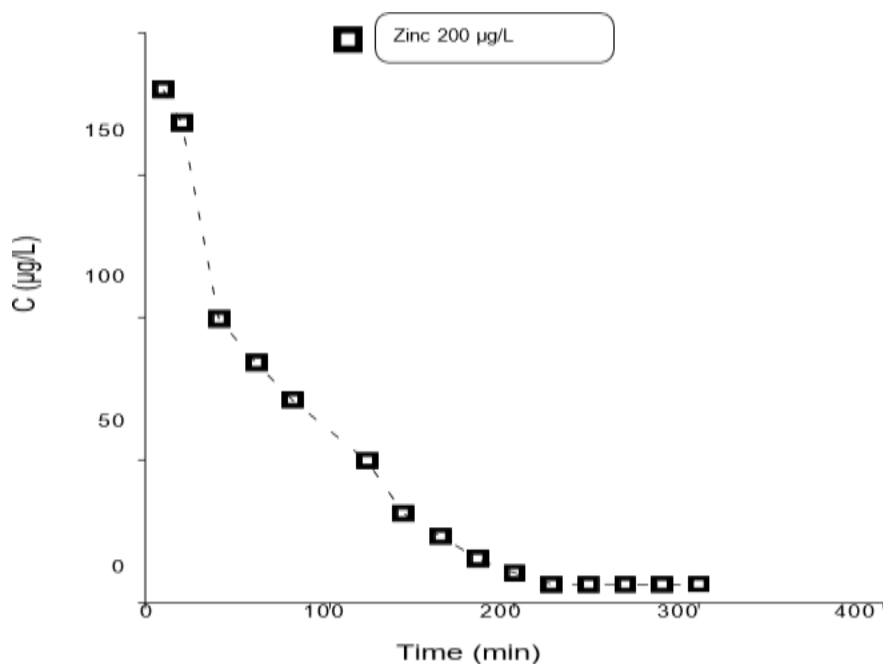
Figure 3.47: Iron oxide nanoparticles synthesised from cantaloupe byproducts and the effect of contact time on zinc adsorption are shown graphically.

3.5 Adsorption thermodynamics

At 30, 40, 50, and 60 degrees Celsius, adsorption experiments were conducted to ascertain the adsorption thermodynamics. The adsorption process's ΔH^0 and ΔS^0 were ascertained using the VantHoff equation. The entropy change is represented by ΔS^0 of, the enthalpy change is represented by K, the temperature in Kelvin is represented by T, and the universal gas constant is represented by R.

$$lnk = \frac{\Delta S^\sim}{R} - \frac{\Delta H}{RT} \quad (3.5)$$

When calculating the value of ΔH0 for the adsorption of arsenic on an adsorbent made from watermelon and melon wastes, the slope was used, and ΔS0 was determined from the intercept of the lnK and 1/T plot. ΔH^0 and ΔS^0 values are listed in table 3.16.

Table 3.16: Enthalpy and Entropy values for the adsorption of heavy metals oniron oxide nanostructures prepared from watermelon and melon waste.

Adsorbent	Heavy metals	ΔH^0	ΔS^0
Watermelon waste	Arsenic	-4.0926	29.156
	Chromium	-9.512	55.742
	Copper	-10.795	54.387
	Lead	-14.721	61.258
	Zinc	-16.645	70.944
Melon waste	Arsenic	-9.093	43.68
	Chromium	-13.112	59.560
	Copper	-13.561	61.487
	Lead	-5.977	29.202
	Zinc	-18.038	72.437

Table 3.17: Gibbs free energy (ΔG^0) values (KJ/mole) for the adsorption of heavy metals on carbon nanostructures prepared from watermelon waste and melon waste.

Adsorbent	Metals	Temperature ( )					
		25	30	35	40	45	50
Watermelon	Arsenic	-8.69	-8.84	-8.98	-9.14	9.28	9.42
	Chromium	-16.62	-16.90	-17.18	-17.46	-17.74	-18.02
	Copper	-16.22	-16.49	-16.77	-17.04	-17.31	-17.58
	Lead	-18.27	-18.58	-18.89	-19.19	-19.50	-19.81
	Zinc	-21.16	-21.52	-21.87	-22.23	-22.58	-22.94
Melon	Arsenic	-13.03	-13.25	-13.46	-13.68	-13.90	-14.12
	Chromium	-17.77	-18.06	-18.36	-18.66	-18.96	-19.25
	Copper	-18.34	-18.65	-18.96	-19.26	-19.57	-19.88
	Lead	-8.71	-8.85	-9.00	-9.15	-9.29	-9.44
	Zinc	-21.61	-21.97	-22.33	-22.70	-23.06	-23.42

Arsenic adsorption on the prepared iron oxide nanostructures is an exothermic process, as shown by the negative (-Ve) values of ΔH^0. On the other hand, the positive value of ΔS^0 from Table 3.16 suggests that the interface between the solid and solution becomes more random during the adsorption process.

$$\Delta G^0 = \Delta H^0 \quad T\Delta S^0 \quad (3.6)$$

The process's spontaneous nature is shown by negative values of ΔG^0 at varying temperatures and by the heavy metals' strong affinity for the produced adsorbents. The values of $\Delta G0$ rise with temperature, indicating that the adsorption process is more favorable for the adsorption of heavy metals at high temperatures as shown in Tale 3.17..

Conclusion

In light of the data of results and discussion, it was determined that adsorbent made from watermelon and melon waste has excellent adsorption capabilities and may be effectively employed as an adsorbent for heavy metal removal.

Ultimately, the study area's drinking water is determined to not provide a chronic health concern. However, as the levels of some of the chosen heavy metals were higher than acceptable, it is advised that the water from polluted locations not be drunk untreated and that the Government of Balochistan, Pakistan, provide alternatives to these regions for drinking water. Melon has been proven to be the most effective food source for heavy metal adsorption when it comes to water melon peel biosorbent materials used in the remediation of heavy metals from water samples. Based on all the data, it can be said that since biosorbent material has a high biosorption capacity, is readily available, and is environmentally acceptable/friendly, it is a more effective option than manufactured biosorbents for removing heavy metals from aqueous solutions.

Recommendations

In order to raise awareness, this research also provides information on the toxicity of heavy metals via polluted drinking water, diagnosis, and uneven access to health care owing to poverty. These quick, affordable, environmentally friendly, and most effective approaches may be employed by scientists and government organizations working on water quality projects or any other project for the evaluation and monitoring of such environmental issues.

In order to remove additional hazardous metals, a natural indigenous biomass was created that is efficient, simple to evaluate, and successful in most cases. The current research yielded baseline data for the comprehensive management of surface and ground water quality, which has a significant impact on the socioeconomic conditions and quality of life of the local people in the studied region.

References

1. Al-Asheh, S., Duvnjak, Z.(**1997)** "Sorption of cadmium and other heavy metals by pine bark" *Journal of Hazardous Materials*, , 56(1), 35-51.
2. Atia, A. A., Donia, A. M., Abou-El-Enein, S. A., Yousif, A. M. (**2003)** "Studies on uptake behavior of copper (II) and lead (II) by amine chelating resins with different textural properties" *Separation and Purification Technology*, 33(3), 295-301.
3. Baby, T.T., Ramaprabhu, S (**2010)** "SiO$_2$ coated Fe$_3$O$_4$ magnetic nanoparticle dispersedmulti walled carbon nanotubes based amperometric glucose biosensor", *Talanta*, 80, 2016–2022.
4. *Baig*, M. I. Bhagwat, V. G.(*2009)* Study the efficacy of GALACTIN VET bolus on milk yield in dairy cows. Vet. World,. 2 (4): 140-142.
5. Bosso, S., Enzweiler, J. (**2002**), "Evaluation of heavy metal removal from aqueous solution onto scolecite" *Water Research*, 36(19), 4795-4800.
6. Campbell, P.G.C., Tessier, A. **(1991)** "Biological availability of metals in sediments analytical approaches, in J. P. Vemet (Ed.) Heavy Metals in the Environment", 161-174.
7. Cheema, A.N., "Management of Water Resources in Pakistan" Proceeding of Firs International Conference, 40th Annual Convention, the Institution of Engineers of Pakistan.

8. Chen, J. (**2002)** "Analysis of water environment in the Xinjiang arid region" *Arid Environ. Monitor*, 16, 223-227.
9. Dieter, H. H., Bayer, T. A., Multhaup, G.(2005), "Environmental copper and manganese in the patho physiology of neurologic diseases (Alzheimer's disease and Manganism) Actahydroch"*Hydrob*" 33, 72–78.
10. Elizabeth, K. M., Naik, L. P. (**2005)** "Water Analysis of Lake Hussain Sagar, Hyderabad, Andhra Pradesh and Bioremediation of Some Pollutants by Fungi" Poll.res, 24(2), 337-340.
11. Emmanuel, E., Pierre, M.G., Perrodin, Y. (**2009)** "Groundwater contamination by microbiological and chemical substances released from hospital wastewater and health risk assessment for drinking water consumers" *Environ. Int*, , 35, 718- 726.
12. Encinar, J.R., and Moldova, M., Lead, in Worsfold, P., Townshend, A. (**2005)** Poole, C.(eds.) *Encyclopedia of Analytical Science*, Elsevier Academic Press: Oxford. p. 56-63.
13. Forstner, U.K., Witman G.T.W. **(1981)** "Metal pollution in the aquatic, Environment" Springer-Verlag Berlin, Heidelberg, 255.
14. Ghoul, M., Bacquet, M., Morcellet, M. **(2003)** "Uptake of heavy metals from synthetic aqueous solutions using modified PEI-silica gels" *Water Research*, 37(4), 729-734.
15. Giles C.H, Macewan T.H, Nakhwa S.N, Smith D (**1960)** "Studies in adsorption. Part IX.
16. Gong, J. L., Wang, X.Y., Zeng, G. M., Chen, L., Deng, J. H., Zhang, X. R., Niu, Q.Y.(**2012)** "Copper (II) removal by pectin–iron oxide magnetic nanocomposite adsorbent",. *Chemical Engineering Journal*, 185–186, 100–107.
17. Groisman, L., Rav-Acha, C., Gerstl, Z., Mingelgrin, U. (**2004)** "Sorption of organic compounds of varying hydro phobicities from water and industrial wastewater by long- and short chain orgnao clays", *Applied Clay Science*, 24, 159–166.
18. Gupta, V. K., Jain, C. K., Ali, I., Sharma, M., Saini, V. K. (**2003)** "Removal of cadmium and nickel from wastewater using bagasse fly ash-a sugar industry waste" *WaterResearch*, 37(16), 4038-4044.
19. Hall, T. M., Waugh, D.W., Boering, K. A., Plumb, R. A., (**1999)** "Evaluation of transport in stratospheric models" *J. Geophys. Res.*,104, 18815-18839.
20. Hayward, K. **(1999)** "Drinking water contaminant hit-list for US EPA" *Water*, 21,4-9.
21. Hu, Z., Lei, L., Li, Y., Ni, Y. (**2003)** "Chromium adsorption on high-performance activated carbons from aqueous solution" *Separation and Purification Technology*, 31(1), 13-18.
22. Kahani S.A, Hamadanian M, Vandadi O (**2007)** "Deposition of Magnetite Nanoparticles in Activated Carbons and Preparation of Magnetic Activated Carbons. Nanotechnology and Its Applications", First Sharjah International Conference. *American Institute of Physics*, , 978-0-7354-0439.
23. Khalown, M.A. **(2004)** "Water Quality Status in Pakistan Report" *PCRWR Islamabad*,
24. Khan, A. T.(**2011)** "Trace elements in the Drinking water and their possible health effects in Aligarh city" *Ind. J. Wat. Res. Prot,* 3, 522-530.
25. Kornaros, M., Lyberatos, G. (**2006)** "Biological treatment of wastewaters from a dye manufacturing company using a trickling filter "*Journal of Hazardous Materials*, 136(1), 95-102.
26. Kumar, A. (**2003)** "Environmental chemistry" 5th Ed, New Age International (P) Limited, , 56-59.
27. Liu, X., Kim, M. **(2009)** "Solvothermal synthesis and magnetic properties of magnetite nanoplatelets.**Materials Letter**, 63:428 - 430.

28. Lopez, F., Martin, M. I., Perez, C., López-Delgado, A., Alguacil, F. J. (**2003**) "Removal of copper ions from aqueous solutions by a steel-making by-product" *Water Research*, 37(16), 3883-3890.

29. Loukidou, M. X., Matis, K. A., Zouboulis, A. I., Liakopoulou-K. M (**2003**) "Removal of As (V) from wastewaters by chemically modified fungal biomass" *Water Research*, 37(18), 4544-4552.

30. Mayur, C. S., PrateekShilpkar and Sangita Sharma (**2007**) Correlation, Regression Study on Physico-chemical parameters and water quality assessment of ground water of Mansa Taluka in Gujarat". *Asian Journal of Chemistry*, 19(5), 3449-3454.

31. *Mishra, A., Bhatt, V., E (**2008**)"Physico-chemical and microbiological analysis of under ground water in VV Nagar and near by places of Anand District, Gujarat, India" J. Chem,, 5(3), 487-492.*

32. Mishra, A., Bhatt, V., Sevak, n., Shah, P., Patel, Patel, C. (**2013**) " Comparative study of physico-chemical and microbial parameters on lotic ,and ground-waters in selected outlying areas of central Gujarat" *Journal of Chemical and Pharmaceutical Research,* 2, 174.

33. Nuria.M,Cesar.V,Ignasi.C,Maria.M and Antonio.F "Cadmium and lead Removal from Aqueous Solution by Grape Stalk Wastes: Modeling of a Fixed Bed Column' Journal of Chemical Engineering Data"**2010,** 55, 3548-3554.

34. Pan, B., Xiong, Y., Su, Q., Li, A. M., Chen, J. L., Zhang, Q. X.(**2003**) "Role of animation of a polymeric adsorbent on phenol adsorption from aqueous solution"*Chemosphere*, 51(9), 953-962.

35. Pereira, M. F. R., Soares, S. F., Orfao, J. M. J., Figueiredo, J. L.(**2003**) "Adsorption of dyes onactivated carbons: influence of surface chemical groups" *Carbon,* , 41, 811-821.

36. Rao, S. M., Mamatha, P.(**2004**) "Water quality in sustainable water management" *Curr. Sci*, , 87, 942.

37. Rapant, S., Krcmova, K. (**2007**) "Health risk assessment maps for arsenic groundwater content, application of national geochemical databases" *Environ. Geochem. Health*, , 29, 131-141.

38. Rivera-Utrilla, J., Bautista-Toledo, I., Ferro-Garca, M. A., Moreno-Castilla, C.(**2003**) "Bioadsorption of Pb (II), Cd (II), and Cr (VI) on activated carbon from aqueous solutions" *Carbon*, , 41(2), 323-330.

39. Robert, G., Mari, G. (**2003**) "Human Health Effects of Metals, US Environmental Protection Agency Risk Assessment Forum" Washington, DC,**.**

40. Robinson, T., Chandran B., Nigam, P.(**2002a**) "Studies on desorption of individual textile dye sand a synthetic dye effluent from dye-adsorbed agricultural residues using solvents" *Bio resource Technology,* 84(3), 299-301.

41. Rodriguez, I., Llompart, M., Cela, R (**2000**) Solid-phase extraction of phenols. *Journal of Chromatography A,* 885(1), 291-304.

42. Rodriguez-Reinoso, F. Activated carbon: structure, characterization, preparation and applications, in Marsh, H.H., Heintz, E.A., Rodriguez-Reinoso, (**1997**) F. (eds.) *Introduction to Carbon Technologies*, Secretariado de Publicaciones: Universidad de Alicante.

43. Safe, S.H.(**1994**) "Polychlorinated biphenyls (PCBs): environmental impact, biochemical and toxic responses, and implications for risk assessment"*CRC Critical Reviews in Toxicology*, 24(2), 87-149.

44. Sarkar, M., Banerjee, A. (**2006**) "ParthaPritam Parameters and Sumit Chakraborty" *Journal of Indian Chemical Society*, 83, 1023-1027.

45. Schwarzenbach, R.P., Egli, T., Hofstetter, T.B., Von Gunten, U., Bernhard W. (**2010)** Global water pollution and human health. *Annual Review of Environment and Resources*, 35, 109-136.

46. Scott, D.V (**2000)** *Advanced Materials for Water Handling: Composites and Thermoplastics*. London: Elsevier.

47. Shen, Y. H. (**2002)** "Removal of phenol from water by adsorption flocculation using organobentonite" *Water Res*, 36, 1107–1114.

48. Singh, V.(**2006)** "Physico-chemical Examination of water, Sewage and Industrial effluents" *Res. J. Chem & ENV*, , 10(3), 62-66.

49. Srinivasan.A and Viraraghavan.T (**2010)** "Decolonization of dye waste waters by biosorbents: A review: *Journal of Environ. Management,* 91, 1915-1929.

50. Strachan, S. (2010) "Heavy metal" *Curr. Anaesth. Crit. Care*, , 21, 44–48.

51. Sundarajan, M., Ramalakshmi, M. (2012) "Novel Cubic Magnetite Nanoparticle Synthesis Using Room Temperature Ionic Liquid", *E-Journal of Chemistry*, 9: 1070-1076.

52. Tanji, K., Valoppi, L. (**1989)** "Ground water contamination by trace elements" *Agri.Ecosys. Environ,* , 26, 239-274.

53. Toth, J. (**1995)** " Thermo dynamical correctness of gas/solid adsorption isotherm Equations". *Journal of Colloidal Interference Science,* 163, 299–302.

54. United Nations Environment Program (UNEP), **1999**. Global Environment Outlook **2000**, Earth scan, UK

55. Vasudevan, P., Padmavathy, V., Dhingra, S. (**2003)** "Kinetics of biosorptionof cadmiumon Baker's yeast*"* Bio resource technology, 89(3), 281-287.

56. Velea, T., Gherghe, L., Predica, V., Krebs, R. (**2009)** "Heavy metal contamination in the vicinity of an industrial area near Bucharest" *Environ. Sci. Pollut. Res*, , 16, S27-S32.

57. Versari, A., Parpinello, G. P., Galassi,S. (2**002)** "Chemometric survey of Italian bottled mineral waters by means of their labelled physico -chemical and chemical composition" *Journal of food composition and analysis,* , 251-268.

58. Wan. W.S.N and Hanfiah. M.A.K.M (**2007)** "Removal of heavy metal ions from wastewater by chemically modified plant wastes as adsorbents: A review, "*Bioresource Technology"*, 99, 3935-3948.

59. Wasserman, G., Liu, X., Parvez, F., Ahsan, H., Levy, D., Litvak, P. F., Kline, J.,Geen, A.V., Slavkovich, V., Lolacono, N., Cheng, Z., Zheng, Y., Graziano, J. (2006) "Water manganese exposure and children's intellectual functions in Araihazar, Bangladesh" *Environ. Health Persp*, 114, 124–129.

60. Wyatt, J., Linton, E.(**1988)** "The industrial potential of microbial nitrile biochemistry" *Cyanide Compounds in Biology*, 32-48.

61. Zahoor M., Khan, F.A. (**2014)** "Adsorption of aflatoxin B1 on magnetic carbon nanostructures prepared from bagasse "*Arabian Journal Chemistry*,

62. Zayed, J., Loranger, S., Kennedy, G. (**1992)** "Variation of trace element concentrations in red spruce tree rings" *Water, Air, and Soil Pollut*, 65(314), 281-291.

63. Zhang, A., Asakura, T., Uchiyama, G. (**2003)** "The adsorption mechanism of uranium (VI) from seawater on a macroporous fibrous polymeric adsorbent containing amidoxime chelating functional group" *Reactive and Functional Polymers*, 57(1), 67-76.